Drug Resistance Updates 79 (2025) 101203

Contents lists available at ScienceDirect

Drug Resistance Updates

journal homepage: www.elsevier.com/locate/drup

Osmotic stress influences microtubule drug response via WNK1 kinase signaling

Ana Monfort-Vengut [a,1], Natalia Sanz-Gómez [a,b,1], Sandra Ballesteros-Sánchez [a,b], Beatriz Ortigosa [a], Aitana Cambón [a], Maria Ramos [c], Ángela Montes-San Lorenzo [a,b], María Escribano-Cebrián [a,b], Juan Manuel Rosa-Rosa [d,e], Joaquín Martínez-López [d,e,f], Ricardo Sánchez-Prieto [b,g,h,i,j,2], Rocío Sotillo [c], Guillermo de Cárcer [b,i,j,*,2]

[a] Cell Cycle & Cancer Biomarkers Laboratory, Cancer Department, Instituto de Investigaciones Biomédicas Sols-Morreale (IIBM) CSIC-UAM, Madrid 28029, Spain
[b] Translational Cancer Research Group, Chronic Diseases and Cancer, Area 3, Instituto Ramón y Cajal de Investigación Sanitaria (IRYCIS), Madrid, Spain
[c] Division of Molecular Thoracic Oncology, German Cancer Research Center (DKFZ), Im Neuenheimer Feld 280, Heidelberg 69120, Germany
[d] Hematology Department, Hospital 12 de Octubre, Madrid 28041, Spain
[e] H12O-CNIO Hematological Tumour Unit, Spanish National Cancer Center (CNIO), Madrid 28029, Spain
[f] Department of Medicine, Complutense University, Madrid 28040, Spain
[g] Molecular Bases of Chemo and Radioresistance in Tumors Laboratory, Cancer Department, Instituto de Investigaciones Biomédicas Sols-Morreale (IIBM) CSIC-UAM, Madrid 28029, Spain
[h] Molecular Oncology Laboratory, Molecular Medicine Unit, Centro Regional de Investigaciones Biomédicas, UCLM, Albacete 02008, Spain
[i] UCLM Biomedicine Unit Associated to CSIC, Spain
[j] CSIC Conexión-Cáncer Hub, Spain

ARTICLE INFO

Keywords:
WNK1
Rigosertib
Microtubule dynamics
Mitosis
Osmotic stress

ABSTRACT

Ion homeostasis is critical for numerous cellular processes, and disturbances in ionic balance underlie diverse pathological conditions, including cancer progression. Targeting ion homeostasis is even considered as a strategy to treat cancer. However, very little is known about how ion homeostasis may influence anticancer drug response. In a genome-wide CRISPR-Cas9 resistance drug screen, we identified and validated the master osmostress regulator WNK1 kinase as a modulator of the response to the mitotic inhibitor rigosertib. Osmotic stress and WNK1 inactivation lead to an altered response not only to rigosertib treatment but also to other microtubule-related drugs, minimizing the prototypical mitotic arrest produced by these compounds. This effect is due to an alteration in microtubule stability and polymerization dynamics, likely maintained by fluctuations in intracellular molecular crowding upon WNK1 inactivation. This promotes resistance to microtubule depolymerizing compounds, and increased sensitivity to microtubule stabilizing drugs. In summary, our data proposes WNK1 osmoregulation activity as an important modulator for microtubule-associated chemotherapy response.

1. Introduction

Targeting mitosis is one of the most efficient strategies to stop cancer cell proliferation (Chan et al., 2012; Dominguez-Brauer et al., 2015; Manchado et al., 2012), and in the last decades a wide variety of new mitotic small compounds were developed targeting essential regulator proteins that govern mitosis progression (polo-like kinases, aurora kinases, NEK kinases, kinesins, etc.) (Henriques et al., 2019; Novais et al., 2021; van Vuuren et al., 2015). Despite many of these new mitotic inhibitors being very efficient in killing cancer cells in vitro, the results from the clinical trials were not successful and none of these compounds are approved for cancer therapy (Komlodi-Pasztor et al., 2012; Yan et al., 2020). A perfect example of this paradigm is the small compound rigosertib (ON-01019). It was originally described as a Plk1 kinase inhibitor, but in recent years it has become clear that rigosertib is a multi-target inhibitor, inhibiting multiple pathways from PI3K-AKT to

* Corresponding author at: Cell Cycle & Cancer Biomarkers Laboratory, Cancer Department, Instituto de Investigaciones Biomédicas Sols-Morreale (IIBM) CSIC-UAM, Madrid 28029, Spain.
E-mail address: gdecarcer@iib.uam.es (G. de Cárcer).
[1] both authors contributed equally.
[2] https://conexion-cancer.csic.es

https://doi.org/10.1016/j.drup.2025.101203
Received 3 September 2024; Received in revised form 17 December 2024; Accepted 7 January 2025
Available online 18 January 2025
1368-7646/© 2025 The Authors. Published by Elsevier Ltd. This is an open access article under the CC BY-NC license (http://creativecommons.org/licenses/by-nc/4.0/).

Table 1
PCR primers with barcodes/indexes used for sgRNA IonTorrent sequencing.

Primer name	Primer sequence (5'-3')
pKLV2_FW	AATGATACGGCGACCACCGAGATCTACACTGGACTATCATATGCTTACCGTAACT
pKLV2_RW Index 1	CAAGCAGAAGACGGCATACGAGATCGTGATGTGACTGGAGTTCAGACGTGTGCTCTTCCGATCTTGCTATGCTGTTTCCAGCAT
pKLV2_RW Index 3	CAAGCAGAAGACGGCATACGAGATGCCTAAGTGACTGGAGTTCAGACGTGTGCTCTTCCGATCTTGCTATGCTGTTTCCAGCAT
pKLV2_RW Index 5	CAAGCAGAAGACGGCATACGAGATCACTGTGTGACTGGAGTTCAGACGTGTGCTCTTCCGATCTTGCTATGCTGTTTCCAGCAT
pKLV2_RW Index 7	CAAGCAGAAGACGGCATACGAGATGATCTGGTGACTGGAGTTCAGACGTGTGCTCTTCCGATCTTGCTATGCTGTTTCCAGCAT

RAS-MEK-ERK signaling, or cellular processes such as microtubule dynamics, with a strong controversy on the precise mechanism of action (Monfort-Vengut and de Carcer, 2023). Despite its efficacy in preclinical studies and the low cytotoxicity shown in clinical trials, rigosertib only showed moderate results in targeting myelodysplastic tumors not reaching the clinical setting (Garcia-Manero et al., 2016). The fact that the exact molecular mechanism is not known, as well as the absence of appropriate biomarkers, may explain the lack of success of rigosertib in the clinic. To define rigosertib biomarkers, we performed a resistance genome-wide CRISPR-Cas9 screen, in the breast cancer cell line MDA-MB-453, and identified the downregulation of the "With-No-lysine [K] kinase 1" (WNK1) as the mayor hit for rigosertib resistance.

WNK1 is a master regulator of ion homeostasis, it controls the influx/efflux of chloride ions upon osmotic stress induction, and it is related to blood pressure control diseases (Deaton et al., 2009; Goldsmith and Rodan, 2023; Richardson and Alessi, 2008; Shekarabi et al., 2017). Chloride ions (Cl^-) are responsible for osmotic pressure and acid-base balance, which determine fundamental biological functions in all tissues (Marunaka, 2023), and impaired Cl^- balance affects several essential cellular processes underlying many pathological conditions, from neuronal excitability to heart failure, cystic fibrosis, or chronic kidney disease (Planells-Cases and Jentsch, 2009). Regarding cancer, ion homeostasis is involved in the proliferation, apoptosis, migration or angiogenesis of cancer cells (Kunzelmann, 2005; Prevarskaya et al., 2010). Importantly, WNK1 is also related to cancer progression (Xiu et al., 2022), and is even considered a putative therapeutic target (Jung et al., 2022; Ye et al., 2024). Although ion homeostasis is also described to influence chemoresistance (Kischel et al., 2019; Wilczynski et al., 2021), little is known about the role of WNK1 in cancer therapy resistance.

Here we describe how WNK1 inactivation leads to rigosertib resistance in breast cancer cell lines, due to alteration in microtubule polymerization dynamics, confirming that rigosertib mainly acts as a microtubule poison. Furthermore, WNK1 downregulation alters the cellular response to general microtubule-related drugs. We propose that WNK1 inactivation, and the subsequent induced osmotic stress, lead to changes in intracellular molecular crowding that alter microtubule polymerization dynamics, conferring resistance to microtubule depolymerizers and sensitivity to microtubule stabilizers.

Table 2
Compound name, vendor source and reference number.

Compound name	Source	Reference
ABT−751	MedChemExpress	HY−13270
Colchicine	Sigma Aldrich	C9754
Danusertib	Selleckchem	S1107
DIDS-sodium salt	MedChemExpress	HY-D0086
Docetaxel	MedChemExpress	HY-B0011
Doxorubicin	Sigma Aldrich	D1515
Doxycycline	BioChemica	A2951
Epothilone A	MedChemExpress	HY−13503
Nocodazole	Selleckchem	S2775
Paclitaxel	Selleckchem	S1150
Rapamicyn	LC Laboratories	R−5000
Rigosertib	MedChemExpress	HY−12037A
Torin1	Selleckchem	S2827
Trametinib	Selleckchem	S2673
Volasertib	Selleckchem	S2235
WNK−463	MedChemExpress	HY−100626
WNK-IN−11	MedChemExpress	HY−112094

2. Material and methods

2.1. Mammalian cell line culture

Cell lines were sourced from the American Type Culture Collection (ATCC®). MDA-MB-453 (RRID:CVCL_0418), MCF-7 (RRID: CVCL_0031), EVSA-T (RRID: CVCL_1207), MDA-MB-231 (RRID: CVCL_0062), HEK-293 (RRID:CVCL_0063), and RPE-1 (RRID: CVCL_4388) cell lines were grown adherently in Dulbecco's Modified Eagle Medium (DMEM) supplemented with 10 % fetal bovine serum (FBS), in a 37ºC and 5 % CO2 atmosphere, and routinely tested for the presence of Mycoplasma species. Cell line authentication was done with the GenePrint® 10 System (Promega), and data were analyzed using GeneMapper® ID-X v1.2 software (Applied Biosystems).

Osmotic stress was induced by either using regular DMEM media for the isoosmotic condition (~335 mOsm/kg); DMEM diluted with 1/3 of milliQ water for the hypoosmotic condition (~225 mOsm/kg) (Serra et al., 2021); or DMEM supplemented with 1.5 % (wt/vol) of 300 Da polyethylene glycol (PEG300) (VWR, VWRC26605.290) for the hyperosmotic condition (~415 mOsm/kg) (Taieb et al., 2021). In all cases, 10 % FBS was added once media were prepared to not interfere with the final growth factor concentration. Media osmolarity was confirmed using a freezing-point osmometer (Gonotec®, Osmomat 010).

2.2. Lentiviral particle generation and cell infection

Third generation lentiviral particles were produced by transfection of HEK-293 cells with a mixture of 10 µg of the lentiviral plasmid of interest, and 6.5 µg, 2.5 µg, and 3.5 µg of the lentiviral packaging vectors (pMDL, pRev, and pVSVg respectively) per p100 plate, using Lipofectamine 2000 (ThermoFisher, 11668019). Cell media was changed 6 h after transfection and cells were incubated at 37º C to allow for virus production. Media containing lentiviral particles was harvested at 48 h and 72 h, filtered through 0.45 µM PVDF membrane filters and flash-frozen at −80º C.

Cell infection was performed by adding lentiviral particles to cell lines in the presence of 8 µg/ml polybrene (Sigma, TR-1003) for 12 h followed by fresh media addition. The selection was further done in the presence of antibiotics such as hygromycin B (50µg/ml), G418 (400µg/ml), or puromycin (2 µg/ml), depending on the selection marker.

2.3. CRISPR-Cas9 genome-wide library generation

TET-ON-Cas9-inducible expressing cells were generated firstly by infection with the rtTA plasmid pLVX-Tet3G (Takara, 631358) and neomycin selection, followed by infection with the U6-sgRNA-TRE-Cas9-P2A-dsRED-EFSGFP/Puro lentiviral particle (LC-TRIP) (Shalem et al., 2014), and puromycin selection, and single-cell cloning to ensure Cas9 expression homogeneity. The sgRNA library, in the pKLV2-U6gRNA5(*Bbs*I)-PGKpuro2ABFP-W plasmid Addgene (#67989) (Tzelepis et al., 2016), was amplified following the detailed protocol described by Koike-Yusa and colleagues (Koike-Yusa et al., 2014), and titrated using Blue Fluorescence Protein (BFP) detection by flow

Table 3
Antibodies used in different applications: WB: Western blot / IF: Immunofluorescence / IHC: immunohistochemistry / FC: flow cytometry.

Antibody (clone)	Source	Reference	Host species	Application	Dilution
alpha-tubulin (DM1A)	Santa Cruz	sc−32293	Mouse	IF / WB	1:2000
gamma-tubulin (GTU88)	Sigma Aldrich	T6557	Mouse	IF	1:1000
acetylated-alpha-tubulin	Sigma Aldrich	T7451	Mouse	IF / WB	1:500
detyrosinated-alpha-tubulin	Sigma Aldrich	AB3201	Rabbit	WB	1:500
histone H3 phospho-S10	Sigma Aldrich	AB3201	Rabbit	IF	1:1000
MDR1	Cell Signaling	#12683	Rabbit	WB	1:500
SPAK	MRC PPU	588713	Sheep	WB	1:2000
SPAK phospho-S373	MRC PPU	588719	Sheep	WB	1:500
WNK1	Invitrogen	PA5–28382	Rabbit	WB	1:500
WNK1	Atlas	HPA046541	Rabbit	FC	1:50
ERK5 phospho-T218/Y220	Cell Signaling	#3371	Rabbit	WB	1:1000
GAPDH (FF26A)	CNIO	-	Mouse	WB	1:10000
vinculin (7F9)	Santa Cruz	sc−73614	Mouse	WB	1:2000
histone H3 phospho-S10	Merck	06–570	Rabbit	IHC	1:200
C3 Cleaved Caspase−3	Cell Signaling	# 9661	Rabbit	IHC	1:300

cytometry (Ruiz et al., 2016). The gRNA library was then transduced in the MDA-MB-453 Cas9-expressing cell line by infecting 30×10^6 cells (100x sgRNA coverage) with a 0.3 multiplicity of infection (MOI) plus polybrene (8 μg/ml) during 2 h. BFP-positive cells were sorted and frozen always keeping a minimum of 10×10^6 cells per cryovial to keep a minimum of 50-fold sgRNA coverage.

2.4. Rigosertib resistance screen

A minimum of 5×10^6 cells (to ensure 50-fold library coverage) of the MDA-MB-4563 cell line CRISPR library were treated with doxycycline (1 μg/ml) for 7 days to induce Cas9 expression and library genetic edition. Cas9 active cells were then treated with rigosertib (100 nM) for 3 days followed by a 4-day holiday period. This protocol was repeated five times until resistant colonies appeared. Once clonal-resistant colonies appeared, 24 resistant colonies were individually isolated and expanded for further analysis. In addition, the rest of the positive colonies were pooled and genomic DNA was extracted for sgRNA enrichment identification

2.5. CRISPR screen sgRNA identification

sgRNA identification in the isolated rigosertib-resistant colonies was done by PCR amplification of the pKLV2 plasmid sgRNA insert region, and PCR product subcloning in the pGEM-T Easy Vector Systems (Promega #A1360) followed by sanger sequencing of pGEM-T positive bacterial colonies. The sgRNA identification, from the pooled resistant cells, was done by PCR amplification of the pKLV2 plasmid sgRNA insert region, using the Q5 High-Fidelity DNA polymerase (NEB, M0491), and the following primers/barcodes (Table 1):

Amplified DNA was purified using AMPure XP Bead-Based Reagent (Beckman Coulter, A63880). For the sequencing library preparation, PCR samples were treated with NEBNext End Repair Module (NEB, E6050) and the adaptor ligated DNA was amplified using NEBNext Q5 Hot Start Hifi PCR Master Mix (NEB, M0543). The libraries were sequenced at a rate of 5 million reads per sample, using the Ion Torrent PGM Platform and the Ion 540 Ampliseq Chip kit (ThermoFisher, A27765).

2.6. WNK1 genetic depletion

WNK1 depletion by CRISPR-Cas9 editing was done by using two independent gRNAs targeting Exon-1 (5'-CGCCGACGCTGTGACCGGC-3') and Exon-4 (5'-ACTTACACTGGTCACGCGA-3') cloned into pKLV2-U6gRNA5(*Bbs*I)-PGKpuro2ABFP-W backbone vector (Addgene #67974). TET-ON-Cas9 expressing cells were infected and BFP-positive cell FACS sorted. WNK1 depletion was done by incubating cells with doxycycline (1 μg/ml) for 7 days. To avoid possible overgrowth of WNK1-WT escapers, WNK1-depleted cells were transiently generated before each experiment. WNK1 edition efficiency was confirmed using the T7-Endonuclease I assay, by PCR amplification of the specific sgRNA target region in the WNK1 locus, exon 1 (FW 5'-GGCTTG TCGGTGCTGAGTG-3' and REV 5'-CTCCCCACAAGGCTAGGCT-3') and exon 4 (FW 5'-GCCCCTGAGATGTATGAGGAG-3' and REV 5'-CCCAACCCCAACAGTTCAC-3'). PCR fragments were incubated with the T7 Endonuclease I (NEB, M0302S) and nuclease activity was confirmed by DNA agarose electrophoresis.

WNK1 genetic indels were identified by pGEM-T subcloning of the same PCR products generated for the T7-endonuclease assay, and positive bacterial colonies were subjected to plasmid DNA sequencing.

WNK1 mRNA silencing was done by using shRNAs lentiviral pLKO plasmids (SIGMA) TRCN0000219718 (5'- TCTGCGGGAAGGCGGTT-TATA-3') and TRCN0000000919 (5'-CCGCGATCTTAAATGTGACAA-3') and puromycin selection for 72 h.

2.7. PiggyBac WNK1 cDNA plasmids cell transfection and selection

WNK1 expressing PiggyBac plasmids (pB-WNK1) were designed and purchased from VectorBuilder GmbH, using the WNK1 cDNA sequence NM_001184985.2, and carrying the blasticidine selection cassette. WNK1 sgRNA targeting sequences at Exon-1 (5'-CGCCGACGCTGT-GACCGGC-3') and Exon-4 (5'-ACTTACACTGGTCACGCGA-3') were mutated to avoid CRISPR edition. A WNK1 kinase death version was generated by mutating Asp368 residue to Ala (D368A) (Xu et al., 2000). MDA-MB-453 cells were transfected either with pB-WNK1-WT or pB-WNK1-D368A cDNAs, together with the Transposase cDNA (GenBank: EF587698) coding plasmid in a 1:5 ratio (PiggyBac plasmid/-transposase plasmid), using Lipofectamine 2000. Transfected cells were then incubated with blasticidine for PiggyBac positive cell selection.

2.8. RNA-seq and qRT-PCR

RNA from control cells or the rigosertib-resistant colonies was extracted with the mirVana miRNA extraction kit (AM1571, Invitrogen) following the manual instructions, and 250 ng with an average RIN= 9.6 (range: 9.4–9.8) in a labchip analysis, were processed into cDNA sequencing libraries with the "QuantSeq 3' mRNA-Seq Library Prep Kit (FWD) for Illumina" (Lexogen, Cat.No. 015). Single-stranded sequencing was carried out with an Illumina NextSeq 500 sequencer obtaining about 10 million reads per sample. Reads were analyzed for quality with FastQC and aligned against the NCBI reference human genome build GRCh38.p13 with HiSat2 (Kim et al., 2019b). Reads were identified with the GTF coordinate file and counted with HTSeq software (Anders et al., 2015). Raw counts were normalized to median ratios in the DeSeq2 package (Love et al., 2014). Differential expression analysis was performed with DeSeq2 comparing rigosertib resistant colonies to control

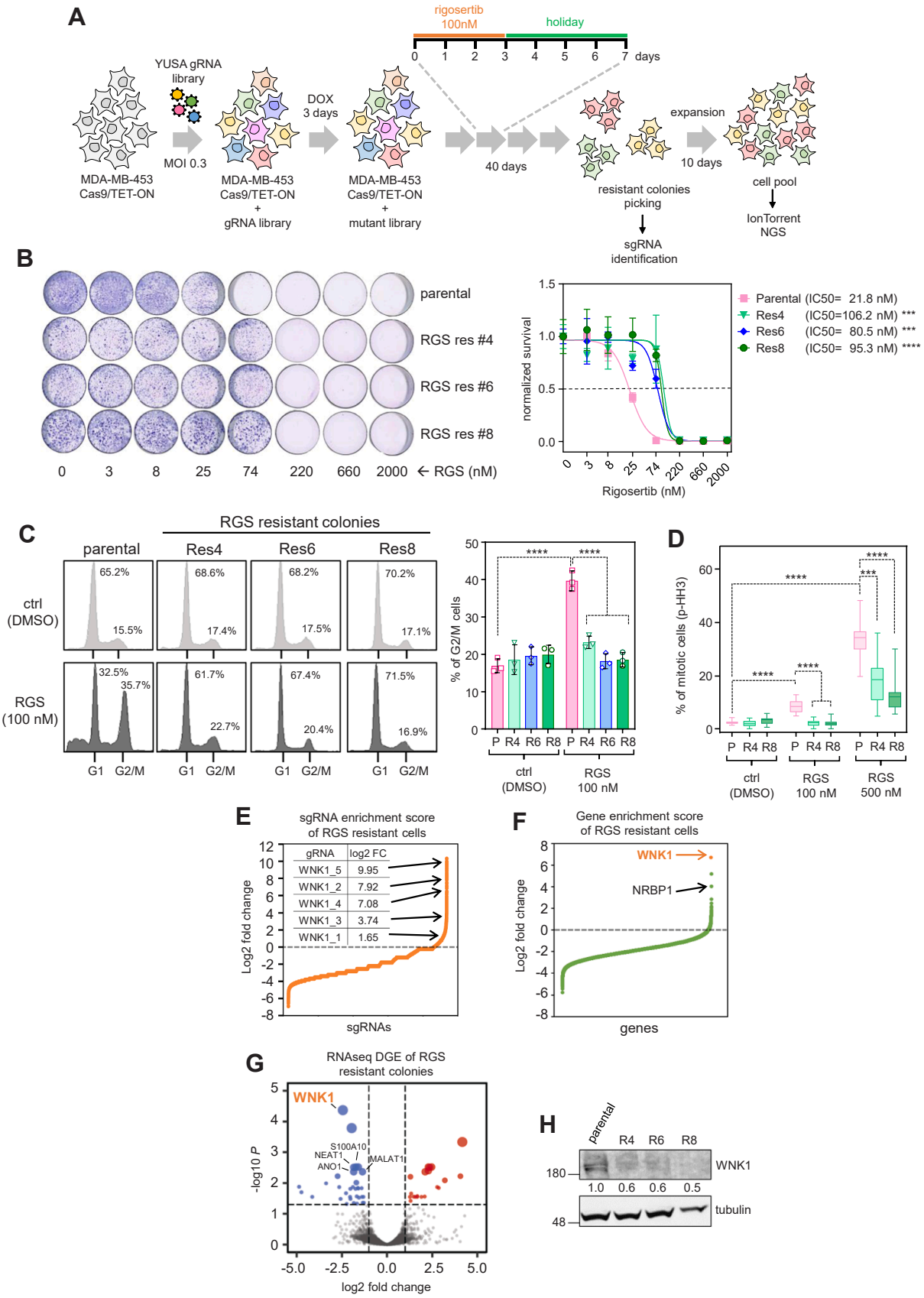

(caption on next page)

Fig. 1. CRISPR-Cas9 screening identifies WNK1 as a hit for rigosertib-acquired resistance: (A) Cartoon summarizing the CRISPR-Cas9 screening process. Three days after Cas9 activation (DOX), the sgRNA library was subjected to 100 nM rigosertib for 3 days followed by 4 days of holiday. This drug regime was repeated five times allowing resistant colonies to appear. Then proliferating colonies were isolated, and the rest of the resistant cells were pooled. (B) Colony formation assays of the isolated rigosertib-resistant colonies (RGS res) in the presence of serial dilutions of rigosertib (left panel), and normalized logarithmic regression plot for rigosertib IC50 calculation of the parental MDA-MB-453 cells (pink line) and the resistant colonies (blue and green lines). Two-way ANOVA with Tukey multiple comparisons test of resistant versus the parental cells: $p < 0.001$ (***) and $p < 0.0001$ (****). Representative graph of three experimental replicates (± SD). (C) Cell cycle profile analysis of parental cells and rigosertib-resistant colonies treated with DMSO (light grey) or 100 nM rigosertib for 16 hours (RGS, dark grey). Numbers within the plots indicate the percentage of cells with G1 or G2/M phases. Histogram on the right represents the average (± SD) of three experimental replicates. (D) Mitotic index quantification by phopho-Ser10 Histone H3 (p-HH3) immunofluorescence in MDA-MB-453 parental cells (P, pink bars) and rigosertib resistant colonies (R, green bars) under 100 nM and 500 nM rigosertib for 16 hours, or DMSO as a control. Five to ten random microscopy fields were quantified per experiment, with more than 500 cells per cohort. Two-way ANOVA (mixed model) with Tukey multiple comparisons test: $p < 0.001$ (***) and $p < 0.0001$ (****). Representative graph of two experimental replicates. (E and F) Waterfall plot showing the enrichment (log2 fold change) of sgRNAs coding for WNK1 (E), and total gene enrichment (F), obtained from deep sequencing of the pooled resistant cells. (G) Volcano plot showing the differential gene expression (DGE) obtained by RNA-seq, comparing three resistant colonies versus the parental MDA-MB-453 cells. Blue dots represent significantly downregulated genes, whereas red dots show upregulated genes. (H) Immunoblot showing the WNK1 protein reduced expression levels in rigosertib-resistant colonies (R), compared to the MDA-MB-453 parental cells. The numbers below each lane indicate the quantification of WNK1 protein levels after normalization to the loading control.

samples, and the volcano plot was generated with the EnhanceVolcano software package. RNA-seq data have been deposited at the Gene Expression Omnibus (GSE271314).

For qRT-PCR, RNA extraction was done using the RNeasy Micro Kit (Qiagen, 74004). cDNA synthesis was done using the QuantiTect Reverse Transcription Kit (Qiagen, 205311). Real-time PCR was done on a starting material of 15 ng of cDNA with SYBR Green PCR Master Mix (Applied Biosystems, 4309155) in a LightCycler II® 480 (Roche), using the WNK1 primers (FW: 5'-CAGAGCCCTGGAATGAACTTG-3', and REV 5'-TTAGGAGGGCTGCTTGTTGC-3') and actin primers (ACTB) as housekeeping gene (FW 5'-TGGATCAGCAAGCAGGAGTATG-3' and REV 5'-GCATTTGCGGTGGACGAT-3').

2.9. Small compounds

Small compounds, listed in Table 2, were used at the doses indicated in figure legends and main text. All compounds were dissolved in DMSO, with the exception of doxycycline that was dissolved in sterile water, and stored at −20º C. To avoid rigosertib degradation, powder aliquots (0.5 mg each) were dark-stored in opaque tubes and conserved at −80ºC. A 1 mM master stock was freshly done for every experimental setting.

2.10. Cell viability assays

Cell growth curves were done by seeding cells in 6-well plates (3×10^5 cells/well) in triplicates and counting every three days using the 3T3 protocol (1/3 dilution every 3 days).

Colony formation assays were done by seeding in 12-well plates (2×10^3 cells/well), or in 24-well plates (1×10^3 cells/well). Drugs were added at the indicated concentrations and renewed every 3–4 days. After 10–14 days, or until the control wells (DMSO) were 80–100 % confluent, cells were fixed with 4 % formaldehyde in PBS, stained with Giemsa, and plates scanned in an Epson V800 scanner. The colony area was quantified using Image J (NIH Bethseda, MD) and its ColonyArea plugin (Guzman et al., 2014). IC50 plots were calculated using the Prism software (GraphPad, Boston, MA).

For the competition assays, cells carrying inducible Cas9 and the WNK1 sgRNAs were infected with either EGFP-expressing lentiviral particles (FUGW-EGFP, Addgene #14883) or FUGW-mRuby3-expressing lentiviral particles (Sanchez-Burgos et al., 2022). EGFP-positive cells were doxycycline treated for 7 days, to deplete the WNK1 gene (WNK1-KD), and then mixed with mRuby3 cells with unedited WNK1 gene (WNK1-WT) at a proportion of 20 %-80 %. 3×10^5 of the cell mixture was seeded in p6 wells by triplicates and incubated in the presence of DMSO or the indicated inhbitors. Cells were grown for 18–29 days with compound renewal every 3–4 days. EGFP vs. mRuby3 proportions were measured by flow cytometry CytoFLEXTM (Beckman Coulter) every 72–96 h by cell suspension in sorting buffer (PBS, 2 % BSA, 1 mM EDTA, 1 mM HEPES pH 7.4).

2.11. Cell cycle profiling

Cell cycle profiling was done by measuring DNA content in the assayed cells by flow cytometry. Trypsinized cells were fixed in slow agitation with cold 70º ethanol and kept on ice for 30 minutes. Then, washed twice with PBS-Triton X-100 0.03 % (Fisher BioReagents, 10102913), and DNA was counterstained with DAPI (1 µg/ml) (AppliChem, A4099) in PBS-Triton X-100 0.03 %. DNA signal was estimated by fluorophore excitation with a 405 nm violet laser and the 450/50 filter in a BD FACSCanto II Flow Cytometer (BD).

2.12. Immunofluorescence and microtubule polymerization assays

Cells growing on coverslips were fixed in 4 % methanol-free formaldehyde (PolySciences, 18814) in PBS and permeabilized with cold methanol. Then, they were blocked with 10 % FBS in PBS-T (PBS, triton-X100 0.03 %) and incubated for 2 h with the primary antibodies, described in Table 3, diluted in PBS-T. Then secondary antibodies, coupled with Alexa488 (green) or Alexa546 (red) dyes (ThermoFisher), were diluted in PBS-T and incubated for 1 h. Finally, DNA was counterstained with DAPI (0.1 µg/ml), and cells were mounted in glass slides using ProLong Diamond antifade mounting media (ThermoFisher, P36965). Pictures were obtained using a Nikon ECLIPSE 90i microscope. For detailed mitotic fate evaluation, pictures were taken with an LSM710 (Zeiss) confocal laser scanning microscope.

The mitotic index was obtained by immunofluorescence staining for phospho-histone H3 (p-HH3) as a mitotic marker and quantifying the percentage of positive p-HH3 in 5–10 random microscopic fields per experiment.

Microtubule polymerization assays were done in RPE-1 cells incubated with the WNK1 inhibitor WNK-463 (5 µM) or DMSO (control) for 24 h. Cells were then chilled over an ice water bath for 30 min, to fully depolymerize the microtubule lattice, and then brought back into warm (37º C) DMEM for 1 min, allowing microtubule regrowth. Immediately, cells were treated for 3 min in CSK buffer (10 mM PIPES/KOH pH 6.8, 100 mM NaCl, 300 mM Sucrose, 1 mM EGTA, 1 mM MgCl2, 1 mM DTT) supplemented with Triton-X100 0.3 % to extract the soluble depolymerized tubulin. Then cells were fixed in absolute cold methanol and stored at −20º C. As a control for the depolymerization assay, some coverslips skipped the ice treatment and were exclusively treated with CSK+ Triton-X100 0.3 % buffer and fixed. Cells were then subjected to alpha- and gamma-tubulin immunofluorescence and microtubule regrowth capacity was quantified by measuring the alpha-tubulin intensity signal in a 20 μm^2 rounded ROI centered at the gamma-tubulin signal, in about 50–100 cells per condition, using ImageJ software program (NIH, Bethesda, MD). The same procedure was followed for WNK1-WT and WNK1-KD MCF-7 cells.

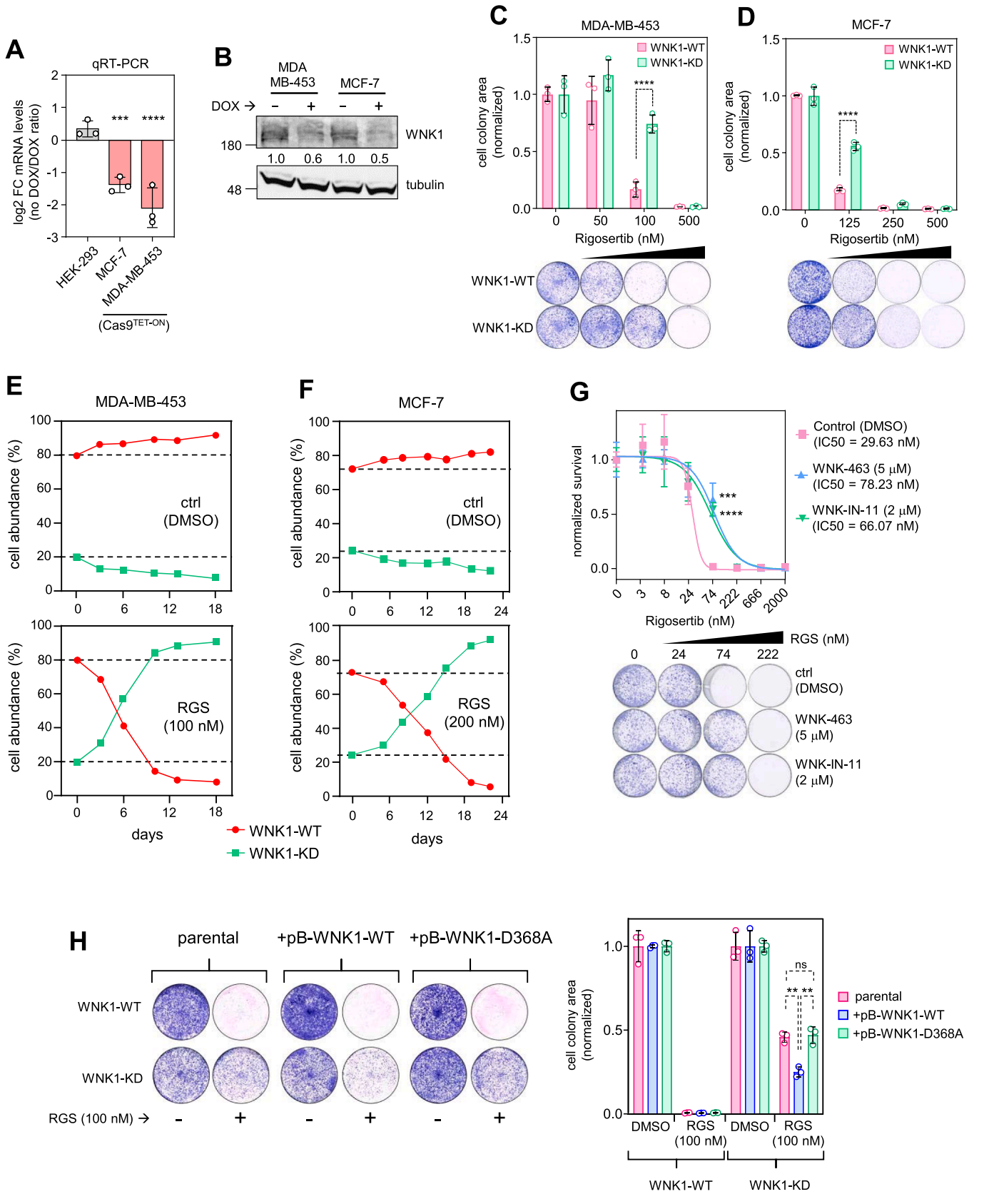

(caption on next page)

Fig. 2. WNK1 inactivation leads to rigosertib resistance: **(A)** WNK1 mRNA expression by qRT-PCR in MCF-7 and MDA-MB-453 cells upon doxycycline (DOX) inducible Cas9 activation ($Cas9^{TET-ON}$). HEK-293 were used as control cells. The plot represents the log2 fold chance ratio of no DOX versus DOX samples. One-way ANOVA with Dunnett's multiple comparison test: $p < 0.001$ (***) and $p < 0.0001$ (****). Representative graph of three experimental replicates. **(B)** Immunoblot showing the reduction of WNK1 protein expression upon genetic depletion (DOX) in MDA-MB-453 and MCF-7 cell lines. The numbers below each lane indicate the quantification of WNK1 protein levels after normalization to the loading control. **(C and D)** Colony formation assay of MDA-MB-453 (**C**) and MCF-7 (**D**) WNK1-WT cells (pink bars) and WNK-KD cells (green bars) in the presence of different concentrations of rigosertib. Two-way ANOVA with Tukey's multiple comparisons test: $p < 0.0001$ (****). Representative graph of three experimental replicates (± SD). **(E and F)** Competition assays of MDA-MB-453 (**E**) and MCF-7 (**F**) WNK1-WT cells (red line) and WNK1-KD cells (green line) under DMSO (top panels) or rigosertib treatment (bottom panels) at the indicated concentrations. **(G)** Colony formation assay and normalized logarithmic regression IC50 calculation of MDA-MB-453 parental cells in the presence of the WNK1 inhibitors WNK-463 (5 μM) (blue line) and WNK-IN-11 (2 μM) (green line), or DMSO as control (pink line), and confronted to serial dilutions of rigosertib. Two-way ANOVA test: $p < 0.001$ (***) and $p < 0.0001$ (****). Representative graph of two experimental replicates **(H)** Colony formation assay of MDA-MB-453 expressing exogenous PiggyBac WNK1 cDNA versions: wild type (+pB-WNK1-WT, blue bars) or kinase death mutant (+pB-WNK1-D368A, green bars); and compared to parental cells (pink bars) in the presence of 100 nM rigosertib. Two-way ANOVA with Tukey's multiple comparisons test: $p < 0.01$ (**). Representative graph of three experimental replicates (± SD).

2.13. EB3-EGFP dynamics analysis by video time-lapse microscopy

RPE-1 cells stably expressing the EB3-EGFP, kindly gifted by Susana A. Godinho (Monteiro et al., 2023), were plated in iBidi 8 multiwell plates and either incubated with the WNK1 inhibitor WNK-463 (5 μM) for 24 hours, paclitaxel (10 nM) for 6 hours, or hyperosmotic media for 24 hours. Then, individual cells were video time-lapsed for 30 seconds, in a Zeiss LSM710 confocal microscope, using a 63 × oil immersion objective lens. EB3-EGFP positive comets were tracked as described by (Matov et al., 2010), quantifying the extension of single EB3 comets for 15 seconds, to calculate the microtubule polymerization speed.

2.14. FRET sensor analysis to measure intracellular molecular crowding

The CRONOS FRET sensor was kindly provided by Kohsuke Kanekura (Miyagi et al., 2021). Briefly, HEK-293 cells were transfected with the CRONOS plasmid using Lipofectamine 2000. 24 hours after transfection, cells were seeded in an iBidi 8-well plate, allowed to attach, and then incubated with the WNK1 inhibitor WNK-463 (5 μM) for 6 hours or with hyperosmotic media for 6 hours. Cells were imaged as described by (Miyagi et al., 2021). Image ratios were calculated using the FRETratioFx tool of the Fiji software (NIH Bethesda, MD).

2.15. Tubulin fractionation, protein lysis and immunoblotting

For MDR1 and WNK1 detection, cells were lysed with Laemmli buffer (2 % SDS, 10 % Glycerol, 60 mM Tris pH 6.8), boiled at 100ºC for 10 min, and centrifuged at 13300 rpm for 15 min. For the rest of proteins, cells were lysed in RIPA buffer (20 mM Tris-HCl pH 7.5, 150 mM NaCl, 1 mM EDTA, 1 mM EGTA, 1 % NP-40, 1 % Sodium deoxycholate) supplemented with 50 U/ml Benzonase® Nuclease (Sigma, #E1014) and 1 % proteases and phosphatases inhibitors (Merck, #P3840; Sigma, #P0044; Sigma, #P5726) on ice for 20 minutes, vortexing every 5 minutes, and centrifuged at 4º C for 15 min at 13300 rpm. Lysate supernatants were quantified for protein concentration using the BCA Protein Assay Kit (TermoFisher Scientific, 23225) and separated on 4–20 % Tris-Glycine gels (NovexTM, Life Technologies). In the case of WNK1, gels were transferred onto PVDF membranes with a constant ampere of 250 mA for 16 h in transfer buffer (Tris/Glycine, 10 % methanol and 0.1 % SDS). For the other antibodies, proteins were transferred onto nitrocellulose membranes using Trans-Blot® TurboTM Transfer System RTA Transfer Kit (BioRad). Blotted membranes were blocked in 10 % non-fat milk in PBS-Tween 20 0.05 % for 30 minutes at room temperature, and then incubated at 4º C overnight with the primary antibody (Table 3). The corresponding secondary antibodies, coupled to fluorescent IRDye680, were incubated for 45 minutes, and scanned with the Odyssey Infrared Imaging System (Li-Cor Biotechnology).

Tubulin soluble/insoluble fractionation assays were done as described in (Giannakakou et al., 2000). Briefly, cells were lysed in Microtubule Solubilizing Buffer (MSB) (1 mM MgCl2, 2 mM EGTA, 0.5 % Nonidet P-40, and 50 mM Tris–HCl (pH 6.8)), supplemented with 1 % proteases and phosphatases inhibitors, during 3 minutes at room temperature. Cells were then centrifuged at 13300 rpm for 10 min at room temperature, and the supernatants containing soluble tubulin were carefully separated from the pellet and flash-frozen in dry ice. Cell pellets were subsequently lysed with Laemmli buffer to obtain the insoluble tubulin fraction. Soluble and insoluble fractions were quantified and analyzed by SDS-PAGE and immunobloted for tubulin

2.16. Mouse xenograft experiments

Mouse tumoral xenograft experiments were done with 8–10 week NMRI female nude mice acquired from Charles Rivers, and they were maintained under standard housing conditions with free access to chow diet and water, as recommended by FELASA (Federation of European Laboratory Animal Science Association). MDA-MB-453 WNK1-WT and WNK1-KD cells were tested for Mycoplasma before engrafting. Briefly, 1×10^6 cells in 100 μl serum-free DMEM were injected in each mouse flank, MDA-MB-453 WNK1-WT in the left flanks and WNK1-KD in the right flanks. When the tumors reached approximately 100 mm^3, they were randomly assigned to rigosertib or vehicle group (6 mice per group), and treatment started with rigosertib sodium salt (300 mg/kg) or the vehicle solution via oral gavage for 5 days followed by 2 days of holiday, during 3 consecutive weeks. Tumors were also measured daily using a caliper and tumor volume was calculated applying the formula: Volume = ½ (Length x $Width^2$). At the end of the treatment, mice were euthanized, and tumors were formalin-fixed and embedded in paraffin. Mice work was performed under the ethical approval protocol G-18/21 from the DKFZ (Heidelberg, Germany) Animal Welfare Office.

To discard rigosertib toxicity, mice weight was measured daily once the compound was administered. In addition, weekly analysis of blood cell populations was performed by extracting fresh blood in K3-EDTA 3 K (Aquisel, 1501126) sample tubes, and analyzed using a hemocytometer (Scil Vet abc Plus, Antech).

2.17. Tumor tissue immunohistochemistry

Mice tumoral tissue paraffin sections were subjected to deparaffinization with xylene and rehydration with graded ethanol. Antigen retrieval was done under 0.09 % (v/v) unmasking solution (Vector Labs) for 30 minutes in a steamer, followed by inactivation of endogenous peroxidases using 3 % hydrogen peroxide (Sigma) for 10 min. Primary antibodies used were phospho-histone H3-Ser10 and C3 cleaved Caspase 3. Specific Alexa fluorophore-labeled goat IgG was used as a secondary antibody, and DAB Peroxidase Substrate kit (Vector Labs) was utilized for antibody detection. Tumor sections were visualized under a Leica DMi1 inverted microscope and analysis of images was performed using ImageJ software program (NIH, Bethesda, MD).

2.18. Statistical analysis

Statistical analysis was performed with the Prism software (GraphPad) using different methods as described in the figure legends. Probabilities of less than 0.05 were considered statistically significant

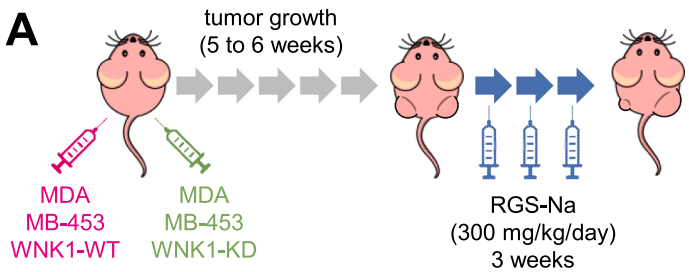

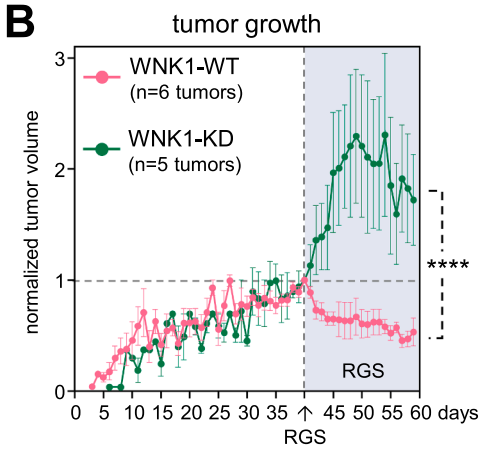

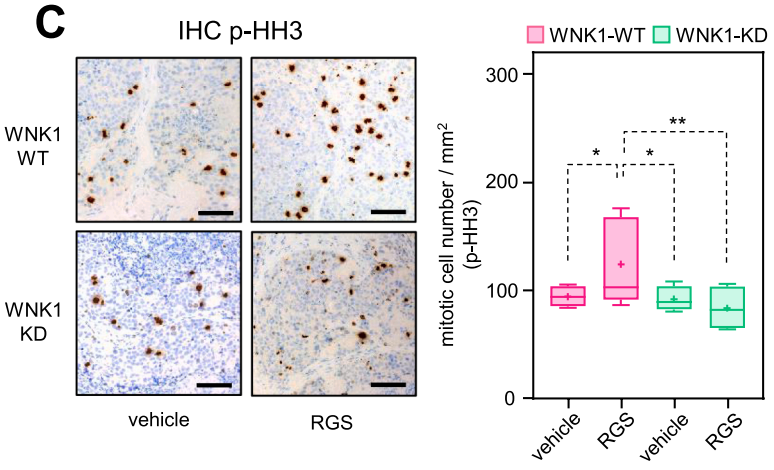

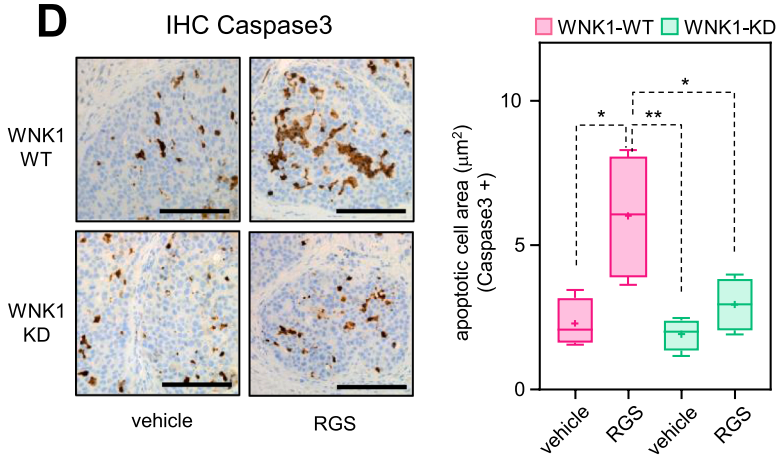

(caption on next page)

Fig. 3. WNK1 inactivation provides survival against rigosertib during in vivo tumoral growth: **(A)** Cartoon of the xenograft experimental design. MDA-MB-453 WNK1-WT and WNK-KD were injected in the left and right flank of nude mice respectively. Once tumors reached approximately 100 mm^3 (5–6 weeks), mice were treated with vehicle or rigosertib sodium salt (RGS-Na). **(B)** Tumor volume growth graph representing the mean (± SD) of WNK1-WT (pink line) and WNK1-KD cells (green line). Tumor volume is normalized on the day of rigosertib administration (blue-shaded area). Two-way ANOVA comparison test of tumoral growth upon rigosertib treatment: $p < 0.0001$ (****). **(C)** Mitotic index detection by immunohistochemistry staining of phospho-Ser10 Histone H3 (p-HH3) (left panel) (bar=100 μM), and percentage of p-HH3 positive cells quantification (right panel) in WNK1-WT (pink bars) and WNK1-KD (green bars) tumors upon rigosertib (RGS) treatment. Two-way ANOVA with Tukey's multiple comparison test of four different tumoral samples per condition: $p < 0.05$ (*), $p < 0.01$ (**) **(D)** Cell death detection by immunohistochemistry staining of cleavage caspase 3 (left panel) (bar=100 μM), and quantification of caspase 3 positive signal area (right panel) in WNK1-WT (pink bars) and WNK1-KD (green bars) tumors upon rigosertib (RGS) treatment. Two-way ANOVA with Tukey's multiple comparison test of four different tumoral samples per condition: $p < 0.05$ (*), $p < 0.01$ (**).

(*$p < 0.05$; **$p < 0.01$; ***$p < 0.001$; ****$p < 0.0001$).

3. Results

3.1. CRISPR-Cas9 screening identifies WNK1 as a determinant for rigosertib response

The Yusa sgRNA library (Tzelepis et al., 2016) was introduced in the breast cancer cell line MDA-MB-453 with inducible expression of Cas9. The sgRNA MDA-MB-453 library was assayed against 100 nM of rigosertib for three days, and a holiday recovery time of four days, repeating this schedule five times until resistant colonies were visible (Fig. 1A, and Supp. Fig. 1A). A collection of 12 resistant colonies was isolated, and the rest of the resistant cells were pulled for further genomic analysis. Isolated resistant colonies were then corroborated to be refractory to rigosertib showing a 3–5-fold increase in the rigosertib IC50 compared to the parental cells (Fig. 1B). None of the isolated rigosertib-resistant cells expressed the multi drug resistant protein (MDR1) (Robey et al., 2018) (Supp. Fig. 1B), and they were as sensitive as the parental cells to other classical anticancer drugs such as the genotoxic agent doxorubicin, the Plk1 mitotic kinase inhibitor volasertib, or the MEK inhibitor trametinib (Supp. Fig. 1C), indicating that cell survival was not based on a general drug resistance mechanism. We also confirmed the acquired resistance by checking the capacity of rigosertib to arrest the cell cycle in mitosis (Gumireddy et al., 2005; Kowalczyk et al., 2021; Radke et al., 2021). Resistant colonies showed no cell cycle arrest in the G2/M cell cycle phase (Fig. 1C), when compared to parental cells, displaying a significant reduction in mitotic arrest as depicted by histone H3 phospho-Ser10 (p-HH3) staining (Fig. 1D).

We then tested the differential enrichment of the sgRNA library in the pooled resistant cells, comparing it to the library with Cas9 activated by doxycycline (DOX) and treated with DMSO, the parental library without Cas9 induction, and the DNA library preparation. The rigosertib-treated cells showed a strong decrease in total sgRNA reads, probably due to massive cell death. Interestingly, there was a significant enrichment in a few reads over the parental controls (Supp. Fig. 1D). The sequence identification showed enrichment of sgRNAs coding for the gene WNK1 (With-No-Lysin [K] 1 kinase), with four WNK1 coding sgRNA, out of the five enclosed in the Yusa library, at the top of the waterfall plot (Fig. 1E). Moreover, when evaluating the sgRNA enrichment by genes, the WNK1 kinase gene was the top hit (Fig. 1F). The presence of WNK1 sgRNA was confirmed in the isolated resistant colonies, mainly detecting the insertion of the sgRNA_5, targeting exon 4, and the sgRNA_2 which targets exon 2 of the WNK1 gene. WNK1 CRISPR edition was verified by T7 endonuclease activity assays (Supp. Fig. 1E), and by sequencing the WNK1 locus indels generated (Supp. Fig. 1F). Worth mentioning, we also found the WNK1 wild-type allele, suggesting that cells cannot completely eliminate WNK1 expression, as it is considered a common essential gene (Supp. Fig. 1G). Indeed, the resistant colonies showed variability in their proliferative index compared to the parental cells (Supp. Fig. 1H), yet they grew efficiently and the proliferative signaling downstream of WNK1 was not impaired, as seen by ERK5 MAP kinase activation (Xu et al., 2004) (Supp. Fig. 1I). Finally, we confirmed the downregulation of WNK1 expression by RNA-seq in three of the isolated colonies compared to the parental cell transcriptome (Fig. 1G), which was also reflected by a strong reduction in WNK1 protein levels (Fig. 1H).

3.2. WNK1 depletion leads to rigosertib treatment resistance

To verify that WNK1 downregulation was responsible for the rigosertib-acquired resistance, we performed specific WNK1 depletion, by CRISPR-Cas9 edition (Supp. Fig. 2A, B) in the MDA-MB-453 and MCF-7 cell lines, as seen by mRNA qRT-PCR (Fig. 2A) and protein expression (Fig. 2B, and Supp. Fig. 2C). WNK1 knocked-down cells (WNK1-KD) have a slightly delayed proliferation rate compared to WNK1-WT cells (Supp. Fig. 3A), yet not impairing cell growth. We then challenged the WNK1-KD cells to grow in the presence of rigosertib, observing increased survival when compared to WNK1-WT cells (Fig. 2C, D). We obtained similar data by WNK1 shRNA downregulation (Supp. Fig. 3B), as well in other cell lines such as EVSA-T and MDA-MB-231 by CRISPR-Cas9 depletion (Supp. Fig. 3C). All these results were corroborated by cell competition assays, mixing WNK1-KD cells (EGFP labeled) and WNK1-WT cells (mRuby3 labeled) in a 20/80 % ratio and culturing them in the presence of rigosertib (Supp. Fig. 3E). DMSO-treated WNK1-KD cells showed a slight reduction in proliferation compared to WNK1-WT cells, whereas under rigosertib treatment, WNK1-KD cells outgrew the culture in approximately one week (MDA-MB-453) to 10 days (MCF-7) and were the only cells detected at the end of the experiment, as almost all WNK1-WT cells were dead (Fig. 2E, F). Furthermore, chemical inhibition of WNK1 kinase activity, using WNK-463 and WNK-IN-11 inhibitors, also protected cells against rigosertib treatment (Fig. 2G), indicating that WNK1 kinase activity is important for efficient cell response to rigosertib.

To further validate these results, we performed rescue experiments in the MDA-MB-453 cell line by expressing a PiggyBac (pB) plasmid carrying the WNK1 cDNA mutated to be resistant to the CRISPR edition, in the wild-type version (pB-WNK1-WT) and a kinase-dead version by mutating the Asp368 residue to Ala (pB-WNK1-D368A) (Xu et al., 2000) (Supp. Fig. 2D). Colony formation assays show a partial but significant rescue of rigosertib sensitivity upon expression of pB-WNK1-WT, whereas pB-WNK1-D368A has the same level of resistance as the parental WNK1-KD cells (Fig. 2H).

Finally, we confirmed that this effect of WNK1 downregulation is replicated in an in vivo context by implanting the MDA-MB-453 WNK1-WT and WNK1-KD cells into nude mice and treating them with either rigosertib sodium salt or vehicle (Fig. 3A). This rigosertib dosing regimen was not toxic, as measured by animal weight and blood cell population counting (Supp. Fig. 4A, B), yet it stopped WNK1-WT tumor growth soon after administration, whereas WNK1-KD tumors were still able to grow (Fig. 3B). Histological analysis of tumors showed a reduction in the mitotic index in WNK1-KD tumors treated with rigosertib (Fig. 3C), confirming the in vitro data from the resistant colonies (Fig. 1D), and a reduction in cleaved caspase-3 staining, when compared to WNK1-WT tumors (Fig. 3D), indicating cell survival.

All of these data demonstrate that WNK1 kinase inactivation mediates acquired resistance to the mitotic inhibitor rigosertib in vitro and in vivo.

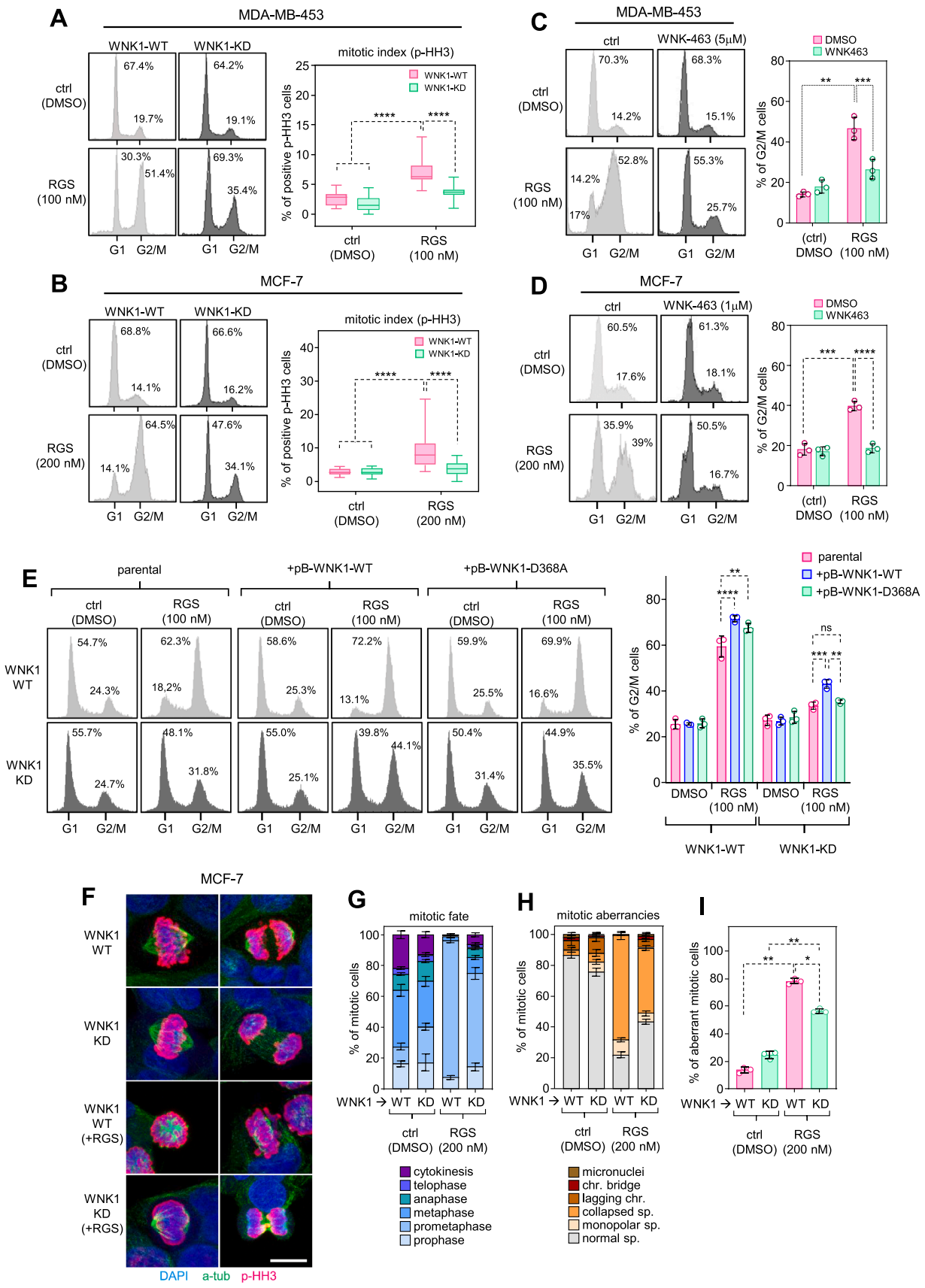

(caption on next page)

Fig. 4. WNK1 inactivation impedes the mitotic arrest mediated by rigosertib. **(A and B)** Cell cycle profile analysis and mitotic index quantification by phospho-Ser10 Histone H3 (p-HH3) of MDA-MB-453 (**A**) and MCF-7 (**B**) WNK1-WT cells (pink bars) and WNK1-KD cells (green bars) treated with rigosertib or DMSO as control for 16 hours. Numbers within the plots indicate the percentage of cells in G1 or G2/M phases. Two-way ANOVA comparison test: $p < 0.0001$ (****). Representative panel of three experimental replicates. **(C and D)** Cell cycle profile analysis of MDA-MB-453 (**A**) and MCF-7 (**B**) WNK1-WT cells incubated with the WNK1 inhibitor WNK-463 (5μM) during 24 hours, and then treated with rigosertib, or DMSO as control, for another 16 hours. Histograms on the right represent the average (± SD) of three experimental replicates. **(E)** Cell cycle profile analysis of WNK1-WT (light grey) and WNK1-KD (dark grey) MDA-MB-453 cells expressing either exogenous PiggyBac WNK1 cDNA constructs: wild-type (+pB-WNK1-WT, blue bars) or kinase-dead mutant (+pB-WNK1-D368A, green bars) and compared with parental cells (pink bars), in the presence of 100 nM rigosertib for 16 hours. Numbers within the plots indicate the percentage of cells with G1 or G2/M phases. Histogram represents the average (± SD) of three experimental replicates. Two-way ANOVA with Tukey's multiple comparison test analysis: $p < 0.01$ (**), $p < 0.001$ (***), $p < 0.0001$ (****). **(F to I)** Mitotic fate study by confocal microscopy of WNK1-WT and WNK1-KD MCF-7 cells, in the presence of rigosertib (200 nM) for 16 hours, and immunostained for α-tubulin (green), phospho-Ser10 histone H3 (red) and DAPI for DNA (blue) (**F**). The mean (± SD) of 100 mitotic cells in each condition was quantified for the different mitotic phases (**G**), different mitotic aberrations (**H**), and total mitotic aberrancies (**I**). Two-way ANOVA with Tukey's multiple comparison test analysis: $p < 0.05$ (*), $p < 0.01$ (**).

3.3. *WNK1 inactivation reduces mitotic arrest upon rigosertib treatment*

Rigosertib is considered a mitotic inhibitor (Gumireddy et al., 2005; Kowalczyk et al., 2021; Radke et al., 2021), and WNK1 kinase has also been shown to modulate mitotic progression, although the underlying mechanism is still unknown (Tu et al., 2011). Thus, we studied the impact of rigosertib and WNK1 inactivation during mitotic progression. WNK1 genetic depletion led to a reduction in mitotic arrest upon rigosertib treatment, both in MDA-MB-453 and MCF-7 cells (Fig. 4A, B) as well in MDA-MB-231 cells (Supp. Fig. 3D). In addition, WNK1 chemical inhibition rendered similar results (Fig. 4C, D), indicating that WNK1 kinase activity impedes the mitotic arrest derived from rigosertib action. It is important to note that the reduction in G2/M arrest is not fully achieved because WNK1 depletion is not complete. Approximately 25 % of the cells still retain WNK1 expression, despite the presence of Cas9 (see Supp. Fig. 2C). This explains why WNK1-KD cells exhibit a significant G2/M arrest when treated with rigosertib, compared to untreated cells. To verify that rigosertib G2/M arrest is dependent on WNK1 activity, we also performed rescue experiments by expressing exogenous WNK1 cDNA in MDA-MB-453 WNK1-KD cells (Fig. 4E). In accordance to the cell survival assays in Fig. 2H, the pB-WNK1-WT cDNA partially rescued the G2/M cell cycle arrest, whereas the pB-WNK1-D368A showed the same level of resistance to rigosertib than parental cells.

A detailed analysis of mitotic progression in MCF-7 WNK1-KD cells (Fig. 4F) showed that there is a slight but not significant increase in mitotic aberrations compared to WNK1-WT cells (Fig. 4I), not enough to induce mitotic arrest, and all phases of mitotic progression can be detected (Fig. 4G). On the other hand, when WNK1-WT cells are treated with rigosertib, there is a dramatic change in the fate of mitotic cells, with almost all cells stacked at the prometaphase stage, with collapsed spindles that are unable to properly align chromosomes, and with no visible advanced phases of mitosis such as anaphase or telophase (Fig. 4G, H). These mitotic aberrations were alleviated in WNK1-KD cells, where we found cells in anaphase and telophase, suggesting that WNK1 inactivation reduces the toxic effect of rigosertib on the mitotic spindle.

3.4. *Inactivation of WNK1 leads to microtubule stabilization, modifying the response to microtubule-associated drugs*

Rigosertib is proposed to be a microtubule-related agent, binding to the α/β-tubulin dimer in the colchicine site, at the interphase of both tubulin monomers. This leads to a microtubule depolymerization causing mitotic progression impairment (Jost et al., 2017, 2020). We, therefore, evaluated if WNK1 depletion could also modify the response to other microtubule depolymerizing ligands such as ABT-751, colchicine, or nocodazole. WNK1-KD cells had a significantly reduced G2/M cell cycle arrest, upon the microtubule depolymerizing compounds treatment, when compared to WNK1-WT cells (Fig. 5A), and this was also reflected in the capacity of WNK1-KD cells to outcompete the WNK1-WT cells when cell proliferation was evaluated by competition assays (Fig. 5B). This indicates that WNK1 inactivation provides survival capacity to other microtubule poisons and it is not a specific mechanism for rigosertib. We also observed a similar response in the rigosertib-resistant colonies isolated from the screening process (Supp. Fig. 5A, C, D). Of note, the impaired response to microtubule depolymerizing drugs was not due to the Leu240Phe mutation in the beta-tubulin gene (TUBB) (Jost et al., 2017) (Supp, Fig. 5E).

Since microtubule-related ligands cause severe mitotic arrest, we wondered whether WNK1 inactivation might synergize with any drug that causes mitotic arrest, regardless of its mechanism of action. Therefore, we tested the response of WNK1-KD cells to other mitotic inhibitors (Fig. 5C). Volasertib (Plk1 kinase inhibitor) and danusertib (Aurora A/B kinase inhibitor) induced a similar G2/M cell cycle arrest in WNK1-WT and WNK1-KD cells, indicating that a mitotic arrest context is not the cause of the differential response of WNK1-KD cells to microtubule poisons. Surprisingly, the Eg5 kinesin inhibitor monastrol resulted in reduced cell cycle arrest in WNK1-KD cells. Eg5 kinesin is not only essential for centrosome separation and mitotic spindle assembly (Mann and Wadsworth, 2019), but is also involved in controlling microtubule dynamics (Freixo et al., 2018; Kim et al., 2019a; Wang et al., 2010), explaining the reduction of cell cycle arrest in WNK1-KD cells, and suggesting that changes in microtubule dynamics are key for the protective effect of WNK1 inactivation against microtubule poisons.

As WNK1 inactivation alters the response to a variety of microtubule-depolymerizing compounds, we wondered if it might also change the response to microtubule-stabilizing drugs such as paclitaxel, epothilone A or docetaxel. In fact, the rigosertib-resistant colonies isolated from the CRISPR screen showed an increased sensitivity to paclitaxel (Supp. Fig. 5B). Similarly, we observed a significant reduction in the survival of MDA-MB-453 WNK-KD cells to paclitaxel compared to WNK1 WT cells (Fig. 5D), which corresponds to an increased arrest in the G2/M phase (Fig. 5E). This effect is also extended to other microtubule-stabilizing compounds such as epothilone A (Fig. 5F, G) and docetaxel (Supp. Fig. 6C), suggesting that WNK1-inactivated cells may have more stable microtubules and therefore require less paclitaxel to achieve a cytotoxic effect.

Overall, WNK1 inactivation influences the response to anti-microtubule drugs, depending on their mode of action (depolymerization or stabilization). We therefore wondered whether WNK1 activity could modulate microtubule dynamics within the cell. To investigate if this was the case, we tested whether WNK1 inactivation could alter the stability of microtubule filaments. MDA-MB-453 and MCF-7 WNK1-KD cells showed elevated levels of acetylated (Ac-α-Tub) and detyrosinated (deTyr-α-Tub) tubulin, two post-traductional modifications concordant with increased stability of the microtubule filaments (Fu et al., 2023; Janke and Montagnac, 2017; Kreis, 1987) (Fig. 6A, B). Noteworthy, the augmented levels of Ac-α-Tub and deTyr-α-Tub were also present in WNK1-KD cells treated with rigosertib or nocodazole, while paclitaxel addition led to a strong signal of both tubulin modifications due to massive stabilization of the microtubules. In addition, we also observed an equivalent increase in Ac-α-Tub staining in RPE-1 cells that were treated with the WNK1 inhibitor WNK-463 (Fig. 6C). The stabilization of tubulin upon depletion of WNK1 can also be observed by tubulin

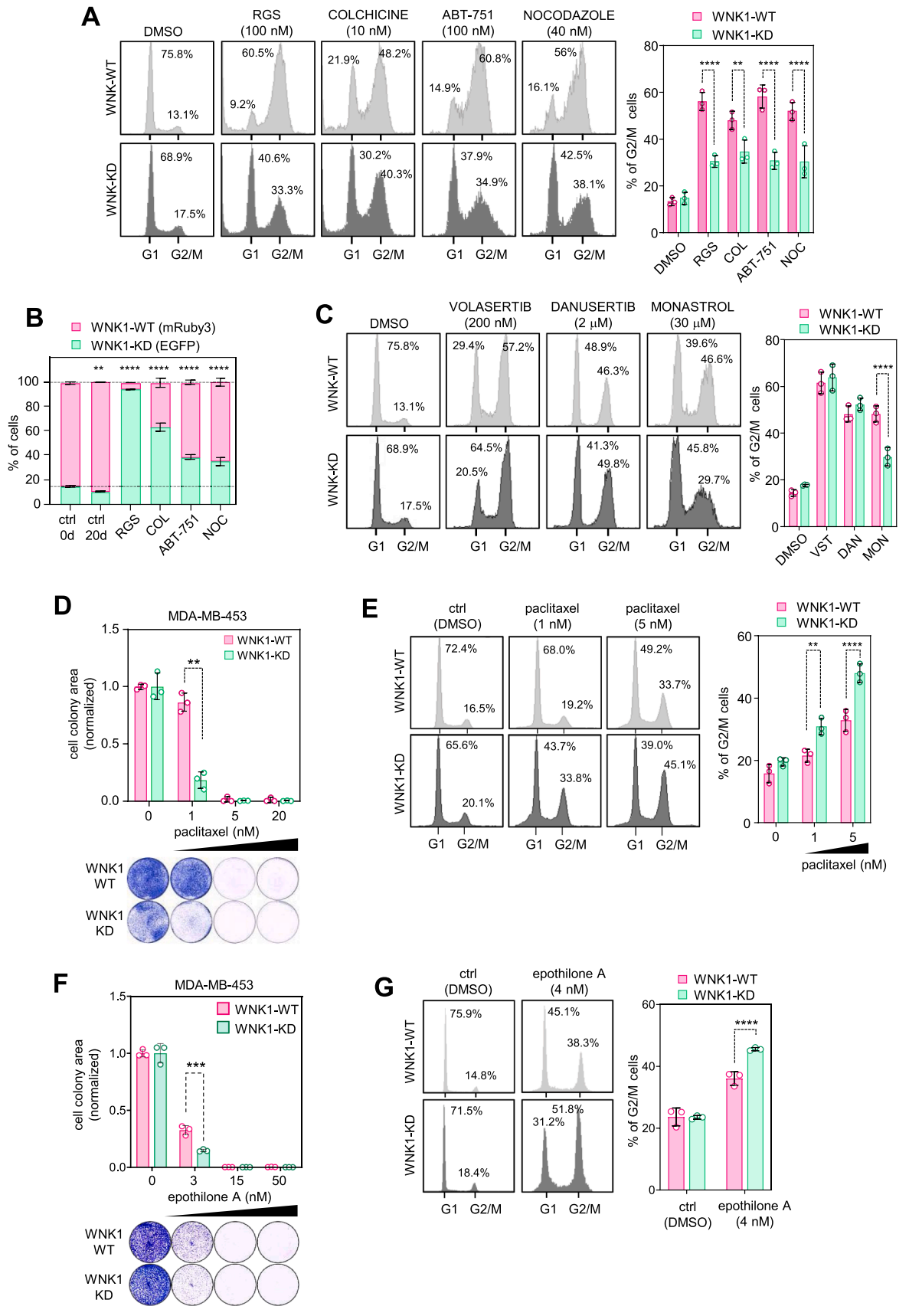

(caption on next page)

Fig. 5. WNK1 inactivation influences the response to microtubule-related compounds: **(A)** Cell cycle profile of MDA-MB-453 WNK1-WT (light grey) and WNK1-KD cells (dark grey) treated with rigosertib, ABT-751, colchicine, and nocodazole for 16 hours at the indicated concentrations. Numbers within the plots indicate the percentage of cells in the G1 and G2/M peaks. Histogram represents the average (± SD) of three experimental replicates. Two-way ANOVA with Tukey's multiple comparison test analysis: $p < 0.01$ (**), $p < 0.0001$ (****). **(B)** Cell competition assay of MDA-MB-453 WNK1-WT (red bars) and WNK1-KD cells (green bars) incubated for 20 days in the presence of 100 nM rigosertib (RGS), 20 nM colchicine (COL), 100 nM ABT-751 and 25 nM nocodazole (NOC). Two-way ANOVA comparison test of the EGFP cell population: $p < 0.01$ (**) and $p < 0.0001$ (****). Representative graph of two experimental replicates (± SD). **(C)** Cell cycle profile of MDA-MB-453 WNK1-WT (light grey) and WNK1-KD cells (dark grey) treated with rigosertib volasertib, danusertib and monastrol for 16 hours, at the indicated concentrations. Numbers within the plots indicate the percentage of cells in the G1 and G2/M peaks. Histogram represents the average (± SD) of three experimental replicates. Two-way ANOVA with Tukey's multiple comparison test analysis: $p < 0.0001$ (****). **(D and F)** Colony formation assays of WNK1-WT (pink bars) and WNK1-KD (green bars) cells incubated with increasing concentrations of paclitaxel (**D**) or epothilone A (**F**). Two-way ANOVA with Tukey's multiple comparison test: $p < 0.01$ (**). Representative graph of three experimental replicates (± SD). **(E and G)** Cell cycle profile of MDA-MB-453 WNK1-WT (light grey) and WNK1-KD cells (dark grey) treated with increasing concentrations of paclitaxel (**E**) or 4 nM epothilone A (**G**) for 16 hours. Numbers within the plots indicate the percentage of cells in the G1 and G2/M peaks. Histogram represents the average of three experimental replicates (± SD). Two-way ANOVA with Tukey's multiple comparison test analysis: $p < 0.01$ (**), $p < 0.0001$ (****).

fractionation experiments in MCF-7 cells (Supp. Fig. 6A). These data suggest that WNK1 inactivation modifies the microtubule dynamics by making them more stable, thus lessening the response to microtubule depolymerizing agents such as rigosertib and others. To verify this hypothesis, we performed classical functional microtubule dynamic assays, by testing the polymerization capacity of tubulin (Ezquerra et al., 2020). RPE-1 cells were incubated with WNK1 inhibitor WNK-463, or DMSO as control, then the microtubule network was depolymerized by cold treatment and allowed to repolymerize in warm media (Fig. 6D). WNK1-inhibited RPE-1 cells showed less microtubule nucleation capacity. The same data was obtained in the MCF-7 cells genetically depleted for WNK1 (Fig. 6E), confirming that WNK1 inactivation alters microtubule polymerization dynamics. Importantly, cold treatment and recovery only affect the microtubule polymerization capacity, since total tubulin levels do not change under the different conditions (Supp. Fig. 6B). We also tested tubulin dynamics by measuring the rate of microtubule polymerization by in vivo tracking the microtubule plus-end protein EB3 fused to EGFP in RPE-1 cells (Fig. 6F, and Supp. Videos related to Fig. 6F). WNK1 inhibition leads to a significant reduction in tubulin polymerization speed (average of 0.23 ± 0.006 μm/sec) compared to untreated cells (average of 0.29 ± 0.009 μm/sec), which is closer to the polymerization speed reduction upon paclitaxel addition (average of 0.18 ± 0.005 μm/sec).

Overall, our data suggest that the WNK1 kinase modulates microtubule dynamics and that WNK1 inactivation confers resistance to microtubule depolymerizing compounds (rigosertib, colchicine, nocodazole) and susceptibility to microtubule stabilizing drugs such as taxanes and epothilones.

3.5. Osmotic stress leads to a differential response of microtubule-associated drugs

WNK1 is a major controller of cellular ion homeostasis, being essential for cells to recover from osmotic stress (Goldsmith and Rodan, 2023). In addition, osmotic stress has been shown to alter the cell cycle and mitotic progression (Funk et al., 2022; Taieb et al., 2021). Therefore, we interrogated if osmotic stress provides a differential response to rigosertib while cells are grown in different osmotic conditions (Fig. 7A, B). Hypoosmotic stress enhanced the rigosertib-mediated G2/M cell cycle arrest in WNK1-WT cells when compared to isoosmotic conditions. Importantly, WNK1-KD cells had a significantly reduced cell cycle arrest (Fig. 7A), and increased survival (Fig. 7B) in both isoosmotic and hypoosmotic conditions, indicating that WNK1 controls the response to rigosertib by counteracting the hypoosmotic stress signaling. Interestingly, cells under hyperosmotic stress did not show any cell cycle arrest upon rigosertib (Fig. 7A), correlating with increased cell survival (Fig. 7B), thus mimicking the inactivation of WNK1.

WNK1 is known to be activated under hypertonic stress (Boyd-Shiwarski et al., 2022; Goldsmith and Huang, 2021), and also under hypotonic stress (Moriguchi et al., 2005; Richardson et al., 2008). All these data are mostly retrieved in short-term osmotic stress experiments (minutes), whereas our osmotic stress assays were done for longer times (days). Thus, we evaluated WNK1 activation signaling under longer osmotic stress induction (3 days), by testing the phosphorylation of the WNK1 effector kinase SPAK (Fig. 7C). In our hands, hypoosmotic stress led to the activating phosphorylation of SPAK in a WNK1-dependent manner, whereas neither hyperosmotic stress nor the presence of rigosertib altered SPAK phosphorylation. These data indicate that hypoosmotic stress activates WNK1 leading to increased sensitivity to rigosertib, while hyperosmotic stress protects against rigosertib by mimicking WNK1 inactivation. In addition, altering the flux of chloride ions, using the ClC-Ka chloride channel blocker DIDS (4, 4′-diisothiocyanato-2,2′-stilbenedisulfonic acid disodium salt) (Wulff, 2008), also provided an increased survival response to rigosertib (Fig. 7D), demonstrating that chloride homeostasis is critical for the response to rigosertib.

Osmotic stress alters microtubule dynamics by modifying the cytoplasm viscosity and increasing the intracellular molecular crowding (Molines et al., 2022). Thus, we tested whether osmotic stress leads to differential response to other microtubule-related compounds. Hypoosmotic stress provided increased sensitivity to microtubule depolymerizing compounds (colchicine and nocodazole) and a less efficient arrest to the microtubule-stabilizing drug paclitaxel (Fig. 8A), as well to docetaxel and epothilone A (Supp. Fig. 6D). On the other hand, hyperosmotic stress provided complete protection to colchicine and nocodazole, whereas paclitaxel, docetaxel, and epothilone A were more efficient in eliciting a G2/M cell cycle arrest (Fig. 8A, and Supp. Fig. 6C). Noteworthy, these changes in drug response were only related to microtubule agents, since the G2/M cell cycle arrest upon Plk1 inhibition (volasertib) or Aurora kinase inhibition (danusertib) did not lead to any differential response associated with osmotic stress (Fig. 8A). Only in the case of hyperosmotic stress, there was a reduction in the G2/M arrest upon Plk1 or Aurora kinases inhibition, but this can be explained by the delay in cell cycle progression under hypertonic stress (Taieb et al., 2021), provoking fewer cells entering into mitosis. Furthermore, we confirmed that hyperosmotic stress alters tubulin dynamics to a similar extent as WNK1 inactivation, as measured by tracking EB3-EGFP comets (Fig. 8B, and Supp. Videos related to Fig. 8B). This result is consistent with reduced Ac-α-Tub levels under hypoosmotic conditions, whereas hyperosmotic stress increases tubulin acetylation similarly to WNK1 inactivation (Fig. 8B), indicating that osmotic stress controls microtubule dynamics via WNK1 signaling.

WNK1 is a sensor for intracellular molecular crowding (Boyd-Shiwarski et al., 2022), and its inactivation leads to elevated cellular macromolecular crowding, mimicking a hyperosmotic stress situation (Xiao et al., 2024). We corroborated this by using the molecular crowding FRET sensor CRONOS (Miyagi et al., 2021) in HEK-293 cells, inactivating WNK1 kinase activity by adding the inhibitor WNK-463, and also incubating the FRET sensor transfected cells in hyperosmotic media (Fig. 8D). Concomitantly, the resistance to rigosertib is rescued when molecular crowding is reduced by inhibiting mTOR signaling (Delarue et al., 2018) (Fig. 8E). Although mTOR

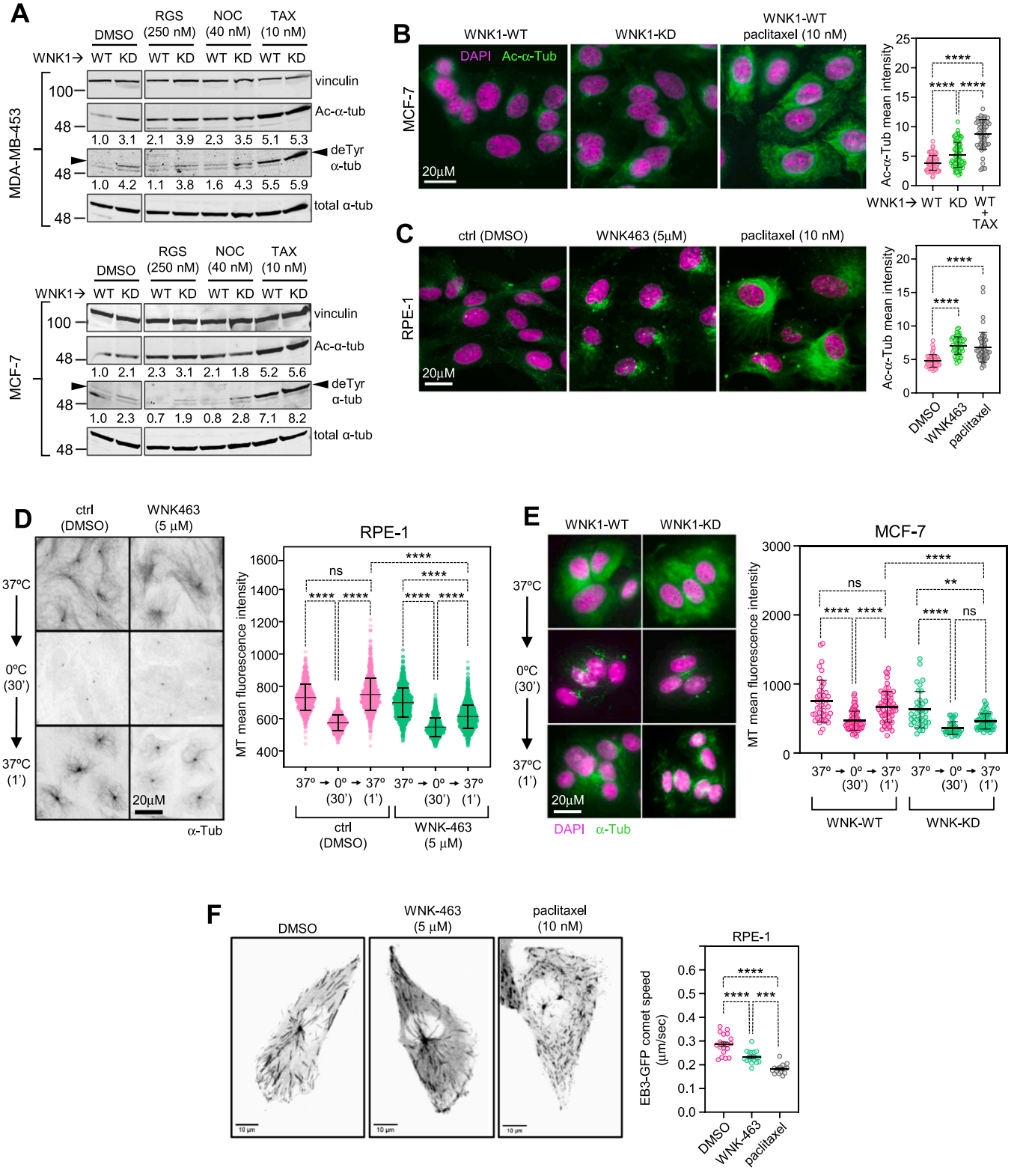

(caption on next page)

Fig. 6. WNK1 inactivation modifies the microtubule polymerization dynamics: **(A)** Biochemical analysis of tubulin stabilization markers by immunoblotting for acetylated alpha-tubulin (Ac-α-tub) and detyrosinated alpha-tubulin (deTyr-α-tub) in MDA-MB-453 (top panel) and MCF-7 (bottom panel) WNK1-WT and WNK1-KD cells treated with rigosertib (RGS), nocodazole (NOC) and paclitaxel (TAX) for 6 hours at the indicated concentrations. Total α-tubulin and vinculin detection were used as loading controls. Numbers below each lane indicate the quantification levels for Ac-α-tub and deTyr-α-tub signal, normalized with the total α-tubulin levels. **(B)** Immunofluorescence staining and quantification of Ac-α-tub levels in WNK1-WT (pink dots) and WNK1-KD (green dots) MCF-7 cells, and WNK1-WT cells incubated with 10 nM paclitaxel for 6 hours (grey dots). Mean (± SD) of 60–100 cells per cohort. One-way ANOVA with Tukey's multiple comparison test: $p < 0.0001$ (****). Bar = 20 μM. **(C)** Immunofluorescence and quantification of Ac-α-tub intensity signal in RPE-1 treated with 5μM WNK-463 (green dots), 10 nM paclitaxel (grey dots), or DMSO as control (pink dots). Mean (± SD) of 50–60 cells per cohort. One-way ANOVA with Tukey's multiple comparison test: $p < 0.0001$ (****). Bar = 20 μM. **(D)** α-tubulin staining images of the microtubule polymerization assay by 30 min ice-cold shock and 1 min recovery in warm (37ºC) media, and mean (± SD) of the α-tubulin intensity quantification plot for over 300 RPE-1 cells treated with WNK-463 (green dots) or DMSO as control (pink dots). Bar = 20 μM. One-way ANOVA with Tukey's comparison test: $p < 0.0001$ (****), and not significant (ns). **(E)** α-tubulin staining images of the microtubule polymerization assay in MCF-7 WNK1-WT (pink dots) and WNK-KD cells (green dots), and mean (± SD) of the α-tubulin intensity quantification plot over 100 cells in each condition. One-way ANOVA with Tukey's comparison test: $p < 0.01$ (**), $p < 0.0001$ (****), and not significant (ns). Bar = 20 μM **(F)** Temporal projections of the videoed EB3-EGFP comet trajectories over 30 seconds, and quantification of the speed rate (μm/sec), in RPE-1 cells treated with 5μM of WNK-463 (green dots) for 24 hours, 10 nM paclitaxel (grey dots) for 6 hours, or DMSO as control (pink dots). An average of 50–150 comets were quantified in each single cell, and 10–20 cells were analyzed in each cohort (± SEM). One-way ANOVA with Tukey's multiple comparison tests: $p < 0.01$ (**), $p < 0.0001$ (****). Bar = 10 μm.

inhibition results in a significant G1 arrest (Chatterjee et al., 2015; Noh et al., 2004) and therefore rigosertib-mediated G2/M arrest was less effective, WNK1-KD cells reached similar G2/M arrest levels as WNK1-WT cells.

Collectively, these data suggest that WNK1 inactivation mimics a hyperosmotic stress situation, increasing intracellular molecular crowding and thus mediating the differential response to microtubule-related drugs by reducing microtubule polymerization dynamics.

4. Discussion

Upon a CRISPR-Cas9 resistance screen for identification of rigosertib-associated biomarkers, we found that inactivation of the osmostress kinase WNK1 mediates cellular resistance to rigosertib (Fig. 1). Using genetic depletion and chemical inhibition approaches, we validated WNK1 as a determinant for rigosertib resistance through in vitro cell proliferation and competition assays, and in vivo xenograft tumor assays (Figs. 2 and 3). Noteworthy, Jost and colleagues (Jost et al., 2017) also found WNK1 as a positive hit in their CRISPR screen for rigosertib response, as depicted from the Open Repository of CRISPR Screens in BioGRID database platform (https://orcs.thebiogrid.org/Screen/1176) (Oughtred et al., 2021), although there is no further description on the possible mechanism behind WNK1 downregulation and rigosertib resistance.

We show that WNK1 inactivation does not modify targeted therapies such as volasertib (Plk1 inhibitor) or trametinib (MEK inhibitor) (Supp. Fig. 1) reinforcing the idea that rigosertib does not act as a RAS-MEK or PLK1 inhibitor in our hands (Jost et al., 2017; Peters et al., 2006). On the contrary, we show that WNK1 inactivation leads to increased microtubule stability, thus not only conferring resistance to rigosertib, but to other similar microtubule poisons such as colchicine, ABT-751 or nocodazole (Fig. 5), and confirming recent data on rigosertib's primary mechanism of action as a microtubule destabilizer (Jost et al., 2017, 2020; Khachatryan et al., 2023). Concomitantly, WNK1 depletion confers sensitivity to microtubule-stabilizing drugs such as paclitaxel or epothilone A, demonstrating that WNK1 activity can modulate microtubule dynamics (Fig. 5). The effect of WNK1 on microtubule dynamics may also explain why WNK1 silencing leads to mitotic aberrations (Tu et al., 2011), although we do not observe such a strong mitotic aberrant phenotype upon WNK1 depletion (Fig. 4), indicating that WNK1 regulation of the mitotic spindle may be cell type-dependent. Importantly, we did not find the Leu240Phe TUBB mutation that confers rigosertib resistance (Jost et al., 2017), hinting a different molecular mechanism for altering tubulin dynamics upon WNK1 inactivation.

WNK1 is a master regulator for the osmotic stress response (Goldsmith and Rodan, 2023) and a sensor of molecular crowding induced by osmotic stress (Boyd-Shiwarski et al., 2022). Interestingly, the CRISPR screen also depicted the NRBP1 gene as a major hit (Fig. 1). NRBP1 is a WNK1 paralog pseudokinase that modulates the activity of the WNK1-SPAK/OSR1 pathway, and it has recently been described as a critical sensor for cell volume homeostasis and molecular crowding (Xiao et al., 2024), thus reinforcing the hypothesis that osmotic stress acts as a modulator for microtubule drug response. Moreover, the rigosertib-resistant colonies show not only strong downregulation of WNK1, but also of other ion homeostasis regulators such as the calcium-activated chloride channel ANO1 (TMEM16A) (Liu et al., 2019), annexin II light chain (S100A10) (Seo and Svenningsson, 2020) or the lncRNAs NEAT1 and MALAT1, both known to be involved in molecular condensation and nuclear speckle crowding (Zacco et al., 2024) (Fig. 1), suggesting that rigosertib-resistant cells have undergone important changes in osmotic stress response signaling. Interestingly, osmotic stress has also been proposed to regulate microtubule dynamics by altering the intracellular molecular crowding and the cytoplasm physicochemical properties (Molines et al., 2022; Shen and Ori-McKenney, 2023). Thus, we evaluated if alterations in cytoplasmic tonicity and crowding, due to osmotic stress, could modify the response to microtubule-associated drugs (Fig. 8). Whereas hypoosmotic stress leads to a more efficient response to microtubule depolymerizing agents and reduces the efficacy of microtubule-stabilizing compounds, hyperosmotic stress has the opposite effect, confirming that imbalances in ion homeostasis can alter the response to microtubule-related drugs. WNK1 inactivation ameliorates these alterations under hypoosmotic stress, having no impact in hyperosmotic conditions. Notably, a recent report showed that WNK1 inhibition indeed leads to cell volume reduction, a significant decrease in intracellular [K+], and the formation of cytoplasmic condensates, all features of hyperosmotic stress (Xiao et al., 2024). Consistent with this, we can eliminate the differential response to rigosertib by reducing molecular crowding using mTOR inhibitors (Fig. 8), suggesting that WNK1 depletion mimics a hyperosmotic scenario leading to increased intracellular molecular crowding, thereby altering microtubule dynamic properties.

Hypoosmotic stress reduces the intracellular chloride levels, while hyperosmosis leads to elevated chloride ions. WNK1 is a chloride sensor that is autoinhibited upon chloride binding, and activated when chloride concentrations are low (Piala et al., 2014). Although WNK1 is classically proposed to be activated by hyperosmotic stress (Boyd-Shiwarski et al., 2022; Goldsmith and Huang, 2021; Zagorska et al., 2007), hypotonic stress can also elicit WNK1 kinase activity (Moriguchi et al., 2005; Richardson et al., 2008). In our experimental setting only hypoosmotic media activates WNK1 (by phospho-SPAK detection) whereas hypertonic stress has very little effect (Fig. 7). These data are consistent with the differential responses to microtubule-associated drugs observed upon osmotic stress induction and WNK1 depletion, confirming that WNK1 controls microtubule dynamics in an osmoregulatory manner.

It is important to mention that the previous studies related to WNK1 activation were performed using short-term osmotic stress induction, while our cell cycle and cell survival assays are conducted over longer times. Worth mentioning, there is a recent report demonstrating that

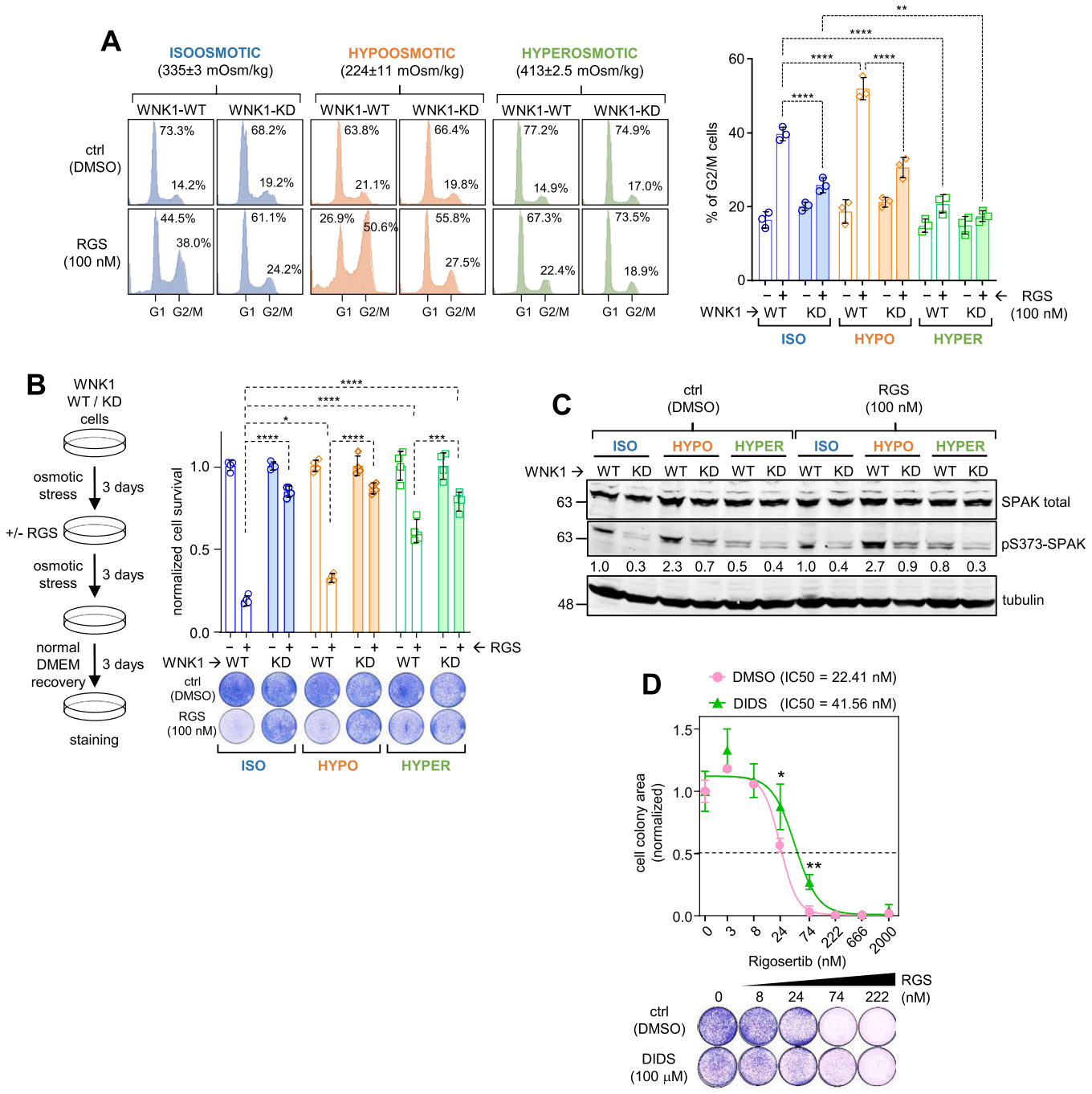

Fig. 7. Osmotic stress-mediated WNK1 signaling results in differential response to rigosertib: **(A)** Cell cycle profile of MDA-MB-453 WNK1-WT and WNK1-KD cells treated with 100 nM rigosertib (RGS) under isoosmotic (blue profiles), hypoosmotic (orange profiles) and hyperosmotic conditions (green profiles). The average of three osmolarity measurements (± SD) are indicated in mOsm/kg. Numbers within the plots show the percentage of cells in the G1 and G2/M peaks. Histogram represents the average (± SD) of three experimental replicates. Two-way ANOVA with Tukey's multiple comparison test analysis: $p < 0.01$ (**), $p < 0.0001$ (****). **(B)** Colony formation assay of MDA-MB-453 WNK1-WT and WNK1-KD cells treated with 100 nM rigosertib (RGS) under different osmotic media conditions. Histogram shows the quantification of cell survival under isoosmotic (blue bars), hypoosmotic (orange bars), and hyperosmotic conditions (green bars), and represents the average (± SD) of two experimental replicates. Two-way ANOVA with Tukey's multiple comparison test: $p < 0.05$ (*), $p < 0.001$ (***), $p < 0.0001$ (****). **(C)** WNK1 signaling analysis by western blot of MDA-MB-453 WNK1-WT and WNK1-KD cells incubated under isoosmotic, hypoosmotic, and hyperosmotic conditions for three days, treated with 100 nM rigosertib (RGS) or DMSO as control for the last 16 hours. Antibodies for total SPAK and phospho-SPAK-Ser373 residue were probed. Tubulin expression was used as loading control. **(D)** Colony formation assay and IC50 calculation of MDA-MB-453 cells grown in the presence of the chloride transport inhibitor DIDS (100μM) (green line), or DMSO as control (pink line), and tested against serial dilutions of rigosertib (RGS). Two-way ANOVA with Tukey's multiple comparison test: $p < 0.05$ (*) and $p < 0.01$ (**). Representative graph of two experimental replicates.

osmotic stress can render long-term effects in cell volume and molecular crowding response, and this seems to be cell dependent (Biswas et al., 2024). Importantly, we confirmed that osmotic stress and WNK1 inactivation indeed lead to increased molecular crowding during several hours (Fig. 8), explaining that osmotic stress can have a long-term impact on cell survival and drug response.

Overall, our data demonstrate that WNK1 activity influences microtubule-associated drug response, and this effect is dependent on

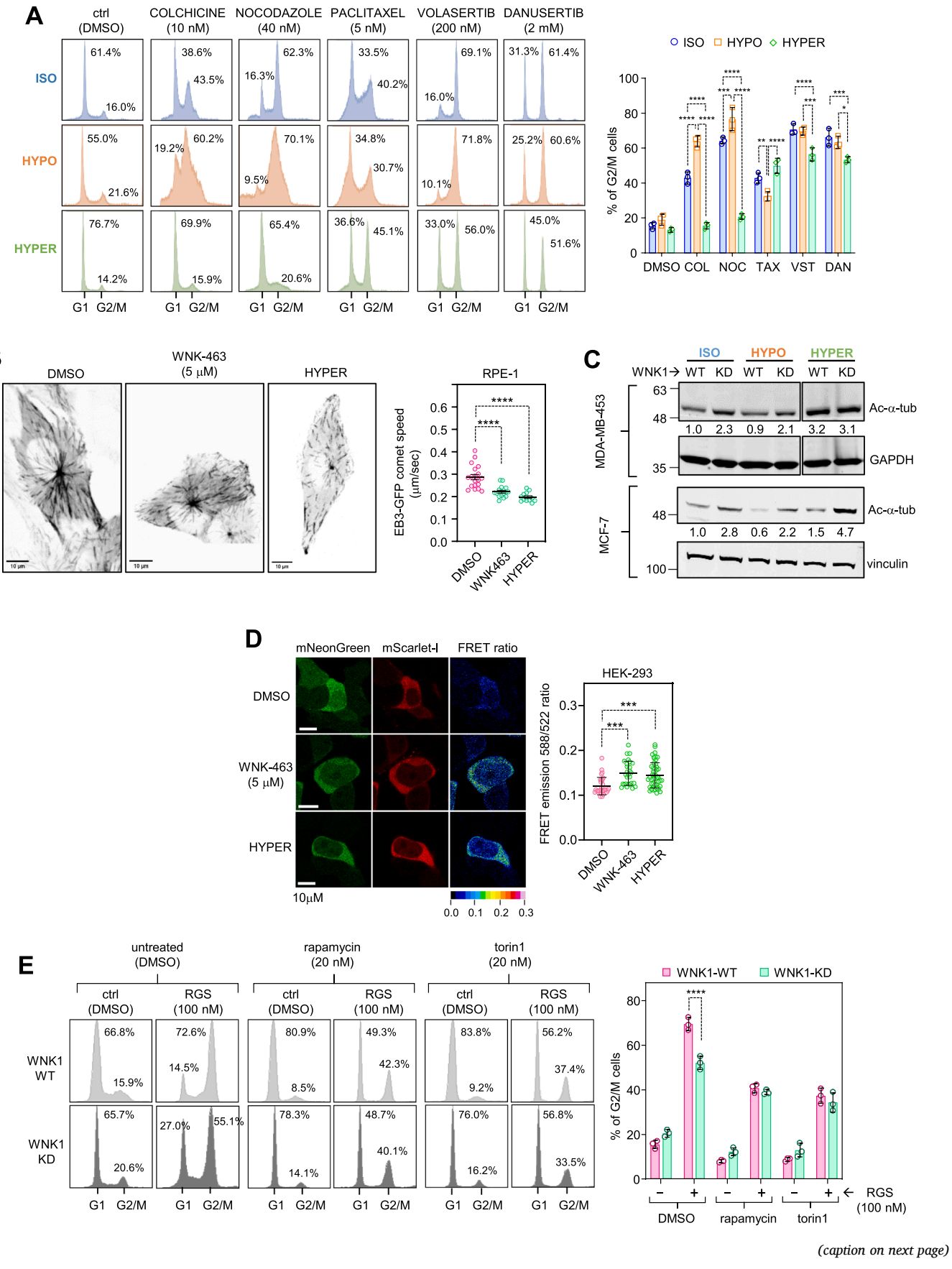

(caption on next page)

Fig. 8. Osmotic stress leads to differential response to microtubule-related compounds: **(A)** Cell cycle profile analysis of MDA-MB-453 cells incubated under iso-osmotic (blue profiles), hypoosmotic (orange profiles), and hyperosmotic (green profiles) media, and treated with the indicated drugs. Numbers within the plots show the percentage of cells in the G1 and G2/M peaks. Histogram represents the average of three experimental replicates. Two-way ANOVA with Tukey's multiple comparison test analysis: $p < 0.05$ (*), $p < 0.001$ (***), $p < 0.0001$ (****). **(B)** Temporal projections of the EB3-EGFP comet trajectories over 30 seconds, and quantification of the speed rate (μm/sec), in RPE-1 cells treated with 5μM WNK-463 for 24 hours, hyperosmotic media for 6 hours (green dots), or DMSO as control (pink dots). An average of 50–150 comets were quantified in each single cell, and 10–20 cells were analyzed in each cohort (± SEM). One-way ANOVA with Tukey's multiple comparison test: $p < 0.0001$ (****). **(C)** Biochemical analysis of acetylated-tubulin (Ac-α-tub) in WNK1-WT and WNK1-KD MDA-MB-453 and MCF-7 cells, incubated for 3 days with either isoosmotic, hypoosmotic or hyperosmotic media. GAPDH or vinculin were used as loading controls. Numbers below each lane indicate the optical density quantification of Ac-α-tub signal, normalized with the loading control levels. **(D)** Intracellular molecular crowding measurement, by using the mNeonGreen-mScarlet-I FRET sensor CRONOS, in HEK-293 cells treated with WNK-463 for 24 hours, hyperosmotic media for 6 hours (green dots), or DMSO as control (pink dots). The average (± SD) of 30–50 cells were analyzed in each cohort. One-way ANOVA with Tukey's multiple comparison test analysis: $p < 0.001$ (***). **(E)** Cell cycle profile analysis of MDA-MB-453 WNK1-WT (light grey) and WNK1-KD (dark grey) cells incubated in with the mTORC inhibitors rapamycin and torin1 during 12 hours, and then tested for cell cycle arrest with 100 nM rigosertib (RGS) for another 16 hours. Numbers within the plots show the percentage of cells in the G1 and G2/M peaks. Histogram represents the average of three experimental replicates. Two-way ANOVA with Tukey's multiple comparison test analysis: $p < 0.0001$ (****).

osmotic stress and the subsequent variations in the intracellular molecular crowding that modify the microtubule polymerization dynamics.

WNK1 has also been described to modulate the dynamics of the actin cytoskeleton (de Boer et al., 2023; Jung and Cobb, 2023; Quelquejay et al., 2024; Zhu et al., 2014), demonstrating that WNK1 can control the cytoskeleton in a variety of actions and suggesting that we cannot rule out other possible mechanisms. For example, the WNK1 downstream osmoregulator SGK1 kinase is known to be a modulator for microtubule dynamics, promoting microtubule depolymerization by phosphorylation of Tau in neurite formation (Yang et al., 2006). Whether this is a conserved mechanism in cancer epithelial cells is yet unknown.

Important to mention, WNK1 abrogation leads to a very strong resistance to rigosertib, that it is not as efficient with other microtubule depolymerizing compounds with similar molecular mode if action like colchicine or ABT-751 (Jost et al., 2017) (Fig. 5). This may be explained by the other possible molecular mechanisms behind rigosertib, especially as an inducer of oxidative stress by activating the JNK-mediated stress cascade (Ritt et al., 2016), and by the fact that WNK1 is also a stress sensor that can modulate JNK signaling (Arai et al., 2020). Although we do not detect WNK1 activation upon rigosertib treatment, this is a possibility worth to explore in the future. Similarly, another report shows that the ability of rigosertib to destabilize microtubules is strongly inhibited by increased levels of uric acid (Rawat et al., 2024). Although the authors here claim that uric acid competes for binding to tubulin, thereby inhibiting the effect of rigosertib, we cannot exclude the possibility of osmotic stress induction due to increased uric acid levels.

In conclusion, our data show that WNK1 kinase, through its function as an osmotic sensor, can alter the response to microtubule-associated drugs. This is clinically relevant and worthy of further investigation in a more clinical scenario, raising a note of caution for cancer patients undergoing chemotherapeutic treatment with microtubule poisons, as disruptions in ion homeostasis may alter the therapeutic efficacy.

CRediT authorship contribution statement

AMV performed the CRISPR screening and most of the experimental procedures, and NSG performed the RNA-seq bioinformatic analysis and important in vitro experiments. BO, SBS, AC, MEC, and AMSL provided technical assistance. AMV, MR and RS participated in and supervised the tumor xenograft experiments. JMRR performed the NGS sequencing and analysis of the CRISPR libraries. JML and RSP provided intellectual input. GdC conceived and supervised the study. All authors participated in the data analysis, and GdC wrote the paper with the help of AMV and NSG.

Declaration of Competing Interest

None of the authors has any conflict of interest.

Acknowledgements

We thank Oscar Fernandez-Capetillo (CNIO), Marcos Malumbres (CNIO/VHIO), Susana Godinho (CRUK), and Kohsuke Kanekura (Tokyo Medical University) for sharing reagents. We also thank Luis del Peso (IIBM-UAM) for helping with the RNA-seq analysis, and Maria Alieva (IIBM) for helping with the video time-lapse microscopy analysis. We thank Monica Martin and Barbara Acosta, at the IIBM Confocal Microscopy Unit, for their technical assistance. This study has been financed by the following grants: From the Ministerio de Ciencia, Innovación, Agencia Estatal de Investigación MCIN/AEI/FEDER UE (doi:10.13039/501100011033): RTI2018–095496-B-I00 and PID2021–125705OB-I00 (GdC); PID2021–122222OB-I00 (RSP); Juan de la Cierva Postdoctoral program FJC2020–044620-I (NSG). From the Spanish Association Against Cancer (AECC) Scientific Foundation: LABAE16017DECA (GdC) and POSTD234371SANZ (NSG). From the Spanish National Research Council (CSIC) with grants 201820I114, 2021-AEP035, 2022–20I018 (GdC), JAEINT_22_01172 (SBS), and JAEINT_24_01201 (MEC). From the UCLM with grant 2022-GRIN-34150 (RSP). EMBO Scientific Exchange Grant (SEG-9883) to AMV, in RS laboratory.

Appendix A. Supporting information

Supplementary data associated with this article can be found in the online version at doi:10.1016/j.drup.2025.101203.

Data availability statement

The RNA-seq data is available at the Gene Expression Omnibus platform (GSE271314). Any other data that support the findings of this study are available from the corresponding author [gdecarcer@iib.uam.es] upon reasonable request.

References

Anders, S., Pyl, P.T., Huber, W., 2015. HTSeq–a Python framework to work with high-throughput sequencing data. Bioinformatics 31, 166–169.

Arai, Y., Asano, K., Mandai, S., Ando, F., Susa, K., Mori, T., Nomura, N., Rai, T., Tanaka, M., Uchida, S., Sohara, E., 2020. WNK1-TAK1 signaling suppresses lipopolysaccharide-induced cytokine production and classical activation in macrophages. Biochem Biophys. Res. Commun. 533, 1290–1297.

Biswas, P., Roy, P., Jana, S., Ray, D., Das, J., Chaudhuri, B., Basunia, R.R., Sinha, B., Sinha, D.K., 2024. Exploring the role of macromolecular crowding and TNFR1 in cell volume control. Elife 13.

Boyd-Shiwarski, C.R., Shiwarski, D.J., Griffiths, S.E., Beacham, R.T., Norrell, L., Morrison, D.E., Wang, J., Mann, J., Tennant, W., Anderson, E.N., Franks, J., Calderon, M., Connolly, K.A., Cheema, M.U., Weaver, C.J., Nkashama, L.J., Weckerly, C.C., Querry, K.E., Pandey, U.B., Donnelly, C.J., Sun, D., Rodan, A.R., Subramanya, A.R., 2022. WNK kinases sense molecular crowding and rescue cell volume via phase separation. Cell 185, 4488–4506 e4420.

Chan, K.S., Koh, C.G., Li, H.Y., 2012. Mitosis-targeted anti-cancer therapies: where they stand. Cell Death Dis. 3, e411.

Chatterjee, A., Mukhopadhyay, S., Tung, K., Patel, D., Foster, D.A., 2015. Rapamycin-induced G1 cell cycle arrest employs both TGF-beta and Rb pathways. Cancer Lett. 360, 134–140.

de Boer, L.L., Vanes, L., Melgrati, S., Biggs O'May, J., Hayward, D., Driscoll, P.C., Day, J., Griffiths, A., Magueta, R., Morrell, A., MacRae, J.I., Kochl, R., Tybulewicz, V.L.J., 2023. T cell migration requires ion and water influx to regulate actin polymerization. Nat. Commun. 14, 7844.
Deaton, S.L., Sengupta, S., Cobb, M.H., 2009. WNK kinases and blood pressure control. Curr. Hypertens. Rep. 11, 421–426.
Delarue, M., Brittingham, G.P., Pfeffer, S., Surovtsev, I.V., Pinglay, S., Kennedy, K.J., Schaffer, M., Gutierrez, J.I., Sang, D., Poterewicz, G., Chung, J.K., Plitzko, J.M., Groves, J.T., Jacobs-Wagner, C., Engel, B.D., Holt, L.J., 2018. mTORC1 controls phase separation and the biophysical properties of the cytoplasm by tuning crowding. Cell 174, 338–349 e320.
Dominguez-Brauer, C., Thu, K.L., Mason, J.M., Blaser, H., Bray, M.R., Mak, T.W., 2015. Targeting mitosis in cancer: emerging strategies. Mol. Cell 60, 524–536.
Ezquerra, A., Viais, R., Luders, J., 2020. Assaying microtubule nucleation. Methods Mol. Biol. 2101, 163–178.
Freixo, F., Martinez Delgado, P., Manso, Y., Sanchez-Huertas, C., Lacasa, C., Soriano, E., Roig, J., Luders, J., 2018. NEK7 regulates dendrite morphogenesis in neurons via Eg5-dependent microtubule stabilization. Nat. Commun. 9, 2330.
Fu, G., Yan, S., Khoo, C.J., Chao, V.C., Liu, Z., Mukhi, M., Hervas, R., Li, X.D., Ti, S.C., 2023. Integrated regulation of tubulin tyrosination and microtubule stability by human alpha-tubulin isotypes. Cell Rep. 42, 112653.
Funk, L., Su, K.C., Ly, J., Feldman, D., Singh, A., Moodie, B., Blainey, P.C., Cheeseman, I. M., 2022. The phenotypic landscape of essential human genes. Cell 185, 4634–4653 e4622.
Garcia-Manero, G., Fenaux, P., Al-Kali, A., Baer, M.R., Sekeres, M.A., Roboz, G.J., Gaidano, G., Scott, B.L., Greenberg, P., Platzbecker, U., Steensma, D.P., Kambhampati, S., Kreuzer, K.A., Godley, L.A., Atallah, E., Collins, Jr, R., Kantarjian, H., Jabbour, E., Wilhelm, F.E., Azarnia, N., Silverman, L.R., O.s. investigators, 2016. Rigosertib versus best supportive care for patients with high-risk myelodysplastic syndromes after failure of hypomethylating drugs (ONTIME): a randomised, controlled, phase 3 trial. Lancet Oncol. 17, 496–508.
Giannakakou, P., Gussio, R., Nogales, E., Downing, K.H., Zaharevitz, D., Bollbuck, B., Poy, G., Sackett, D., Nicolaou, K.C., Fojo, T., 2000. A common pharmacophore for epothilone and taxanes: molecular basis for drug resistance conferred by tubulin mutations in human cancer cells. Proc. Natl. Acad. Sci. USA 97, 2904–2909.
Goldsmith, E.J., Huang, C.L., 2021. LRRC8A reduces intracellular chloride to permit WNK activation in response to hypertonic stress. Proc. Natl. Acad. Sci. USA 118.
Goldsmith, E.J., Rodan, A.R., 2023. Intracellular ion control of WNK signaling. Annu Rev. Physiol. 85, 383–406.
Gumireddy, K., Reddy, M.V., Cosenza, S.C., Boominathan, R., Baker, S.J., Papathi, N., Jiang, J., Holland, J., Reddy, E.P., 2005. ON01910, a non-ATP-competitive small molecule inhibitor of Plk1, is a potent anticancer agent. Cancer Cell 7, 275–286.
Guzman, C., Bagga, M., Kaur, A., Westermarck, J., Abankwa, D., 2014. ColonyArea: an ImageJ plugin to automatically quantify colony formation in clonogenic assays. PLoS One 9, e92444.
Henriques, A.C., Ribeiro, D., Pedrosa, J., Sarmento, B., Silva, P.M.A., Bousbaa, H., 2019. Mitosis inhibitors in anticancer therapy: when blocking the exit becomes a solution. Cancer Lett. 440-441, 64–81.
Janke, C., Montagnac, G., 2017. Causes and consequences of microtubule acetylation. Curr. Biol. 27, R1287–R1292.
Jost, M., Chen, Y., Gilbert, L.A., Horlbeck, M.A., Krenning, L., Menchon, G., Rai, A., Cho, M.Y., Stern, J.J., Prota, A.E., Kampmann, M., Akhmanova, A., Steinmetz, M.O., Tanenbaum, M.E., Weissman, J.S., 2017. Combined CRISPRi/a-based chemical genetic screens reveal that rigosertib is a microtubule-destabilizing agent. Mol. Cell 68, 210–223 e216.
Jost, M., Chen, Y., Gilbert, L.A., Horlbeck, M.A., Krenning, L., Menchon, G., Rai, A., Cho, M.Y., Stern, J.J., Prota, A.E., Kampmann, M., Akhmanova, A., Steinmetz, M.O., Tanenbaum, M.E., Weissman, J.S., 2020. Pharmaceutical-grade rigosertib is a microtubule-destabilizing agent. Mol. Cell 79, 191–198 e193.
Jung, J.U., Cobb, M.H., 2023. WNK1 controls endosomal trafficking through TRIM27-dependent regulation of actin assembly. Proc. Natl. Acad. Sci. USA 120, e2300310120.
Jung, J.U., Jaykumar, A.B., Cobb, M.H., 2022. WNK1 in malignant behaviors: a potential target for cancer? Front. Cell Dev. Biol. 10, 935318.
Khachatryan, H., Olszowy, B., Barrero, C.A., Gordon, J., Perez-Leal, O., 2023. Identification of inhibitors of tubulin polymerization using a crispr-edited cell line with endogenous fluorescent tagging of beta-tubulin and histone H1. Biomolecules 13.
Kim, C.D., Kim, E.D., Liu, L., Buckley, R.S., Parameswaran, S., Kim, S., Wojcik, E.J., 2019a. Small molecule allosteric uncoupling of microtubule depolymerase activity from motility in human Kinesin-5 during mitotic spindle assembly. Sci. Rep. 9, 19900.
Kim, D., Paggi, J.M., Park, C., Bennett, C., Salzberg, S.L., 2019b. Graph-based genome alignment and genotyping with HISAT2 and HISAT-genotype. Nat. Biotechnol. 37, 907–915.
Kischel, P., Girault, A., Rodat-Despoix, L., Chamlali, M., Radoslavova, S., Abou Daya, H., Lefebvre, T., Foulon, A., Rybarczyk, P., Hague, F., Dhennin-Duthille, I., Gautier, M., Ouadid-Ahidouch, H., 2019. Ion channels: new actors playing in chemotherapeutic resistance. Cancers 11.
Koike-Yusa, H., Li, Y., Tan, E.P., Velasco-Herrera Mdel, C., Yusa, K., 2014. Genome-wide recessive genetic screening in mammalian cells with a lentiviral CRISPR-guide RNA library. Nat. Biotechnol. 32, 267–273.
Komlodi-Pasztor, E., Sackett, D.L., Fojo, A.T., 2012. Inhibitors targeting mitosis: tales of how great drugs against a promising target were brought down by a flawed rationale. Clin. Cancer Res. 18, 51–63.
Kowalczyk, J.T., Wan, X., Hernandez, E.R., Luo, R., Lyons, G.C., Wilson, K.M., Gallardo, D.C., Isanogle, K.A., Robinson, C.M., Mendoza, A., Heske, C.M., Chen, J.Q., Luo, X., Kelly, A.E., Difilippantinio, S., Robey, R.W., Thomas, C.J., Sackett, D.L., Morrison, D.K., Randazzo, P.A., Jenkins, L.M.M., Yohe, M.E., 2021. Rigosertib induces mitotic arrest and apoptosis in RAS-mutated rhabdomyosarcoma and neuroblastoma. Mol. Cancer Ther. 20, 307–319.
Kreis, T.E., 1987. Microtubules containing detyrosinated tubulin are less dynamic. EMBO J. 6, 2597–2606.
Kunzelmann, K., 2005. Ion channels and cancer. J. Membr. Biol. 205, 159–173.
Liu, Y., Zhang, H., Men, H., Du, Y., Xiao, Z., Zhang, F., Huang, D., Du, X., Gamper, N., Zhang, H., 2019. Volume-regulated Cl(-) current: contributions of distinct Cl(-) channels and localized Ca(2+) signals. Am. J. Physiol. Cell Physiol. 317, C466–C480.
Love, M.I., Huber, W., Anders, S., 2014. Moderated estimation of fold change and dispersion for RNA-seq data with DESeq2. Genome Biol. 15, 550.
Manchado, E., Guillamot, M., Malumbres, M., 2012. Killing cells by targeting mitosis. Cell Death Differ. 19, 369–377.
Mann, B.J., Wadsworth, P., 2019. Kinesin-5 regulation and function in mitosis. Trends Cell Biol. 29, 66–79.
Marunaka, Y., 2023. Physiological roles of chloride ions in bodily and cellular functions. J. Physiol. Sci. 73, 31.
Matov, A., Applegate, K., Kumar, P., Thoma, C., Krek, W., Danuser, G., Wittmann, T., 2010. Analysis of microtubule dynamic instability using a plus-end growth marker. Nat. Methods 7, 761–768.
Miyagi, T., Yamanaka, Y., Harada, Y., Narumi, S., Hayamizu, Y., Kuroda, M., Kanekura, K., 2021. An improved macromolecular crowding sensor CRONOS for detection of crowding changes in membrane-less organelles under stressed conditions. Biochem Biophys. Res. Commun. 583, 29–34.
Molines, A.T., Lemiere, J., Gazzola, M., Steinmark, I.E., Edrington, C.H., Hsu, C.T., Real-Calderon, P., Suhling, K., Goshima, G., Holt, L.J., Thery, M., Brouhard, G.J., Chang, F., 2022. Physical properties of the cytoplasm modulate the rates of microtubule polymerization and depolymerization. Dev. Cell 57, 466–479 e466.
Monfort-Vengut, A., de Carcer, G., 2023. Lights and shadows on the cancer multi-target inhibitor rigosertib (ON-01910.Na). Pharmaceutics 15.
Monteiro, P., Yeon, B., Wallis, S.S., Godinho, S.A., 2023. Centrosome amplification fine tunes tubulin acetylation to differentially control intracellular organization. EMBO J. 42, e112812.
Moriguchi, T., Urushiyama, S., Hisamoto, N., Iemura, S., Uchida, S., Natsume, T., Matsumoto, K., Shibuya, H., 2005. WNK1 regulates phosphorylation of cation-chloride-coupled cotransporters via the STE20-related kinases, SPAK and OSR1. J. Biol. Chem. 280, 42685–42693.
Noh, W.C., Mondesire, W.H., Peng, J., Jian, W., Zhang, H., Dong, J., Mills, G.B., Hung, M. C., Meric-Bernstam, F., 2004. Determinants of rapamycin sensitivity in breast cancer cells. Clin. Cancer Res. 10, 1013–1023.
Novais, P., Silva, P.M.A., Amorim, I., Bousbaa, H., 2021. Second-generation antimitotics in cancer clinical trials. Pharmaceutics 13.
Oughtred, R., Rust, J., Chang, C., Breitkreutz, B.J., Stark, C., Willems, A., Boucher, L., Leung, G., Kolas, N., Zhang, F., Dolma, S., Coulombe-Huntington, J., Chatr-Aryamontri, A., Dolinski, K., Tyers, M., 2021. The BioGRID database: a comprehensive biomedical resource of curated protein, genetic, and chemical interactions. Protein Sci. 30, 187–200.
Peters, U., Cherian, J., Kim, J.H., Kwok, B.H., Kapoor, T.M., 2006. Probing cell-division phenotype space and Polo-like kinase function using small molecules. Nat. Chem. Biol. 2, 618–626.
Piala, A.T., Moon, T.M., Akella, R., He, H., Cobb, M.H., Goldsmith, E.J., 2014. Chloride sensing by WNK1 involves inhibition of autophosphorylation. Sci. Signal 7, ra41.
Planells-Cases, R., Jentsch, T.J., 2009. Chloride channelopathies. Biochim Biophys. Acta 1792, 173–189.
Prevarskaya, N., Skryma, R., Shuba, Y., 2010. Ion channels and the hallmarks of cancer. Trends Mol. Med. 16, 107–121.
Quelquejay, H., Al-Rifai, R., Silvestro, M., Vandestienne, M., Ferreira, I., Mirault, T., Henrion, D., Zhong, X., Santos-Zas, I., Goudot, G., Alayrac, P., Robidel, E., Autret, G., Balvay, D., Taleb, S., Tedgui, A., Boulanger, C.M., Zernecke, A., Saliba, A.E., Hadchouel, J., Ramkhelawon, B., Cochain, C., Bergaya, S., Jeunemaitre, X., Ait-Oufella, H., 2024. L-Wnk1 deletion in smooth muscle cells causes aortitis and inflammatory shift. Circ. Res. 135, 488–502.
Radke, K., Hansson, K., Sjolund, J., Wolska, M., Karlsson, J., Esfandyari, J., Pietras, K., Aaltonen, K., Gisselsson, D., Bexell, D., 2021. Anti-tumor effects of rigosertib in high-risk neuroblastoma. Transl. Oncol. 14, 101149.
Rawat, V., DeLear, P., Prashanth, P., Ozgurses, M.E., Tebeje, A., Burns, P.A., Conger, K. O., Solis, C., Hasnain, Y., Novikova, A., Endress, J.E., Gonzalez-Sanchez, P., Dong, W., Stephanopoulos, G., DeNicola, G.M., Harris, I., Sept, D., Mason, F.M., Coloff, J.L., 2024. Drug screening in human physiologic medium identifies uric acid as an inhibitor of rigosertib efficacy. JCI Insight.
Richardson, C., Alessi, D.R., 2008. The regulation of salt transport and blood pressure by the WNK-SPAK/OSR1 signalling pathway. J. Cell Sci. 121, 3293–3304.
Richardson, C., Rafiqi, F.H., Karlsson, H.K., Moleleki, N., Vandewalle, A., Campbell, D.G., Morrice, N.A., Alessi, D.R., 2008. Activation of the thiazide-sensitive Na+ -Cl- cotransporter by the WNK-regulated kinases SPAK and OSR1. J. Cell Sci. 121, 675–684.
Ritt, D.A., Abreu-Blanco, M.T., Bindu, L., Durrant, D.E., Zhou, M., Specht, S.I., Stephen, A.G., Holderfield, M., Morrison, D.K., 2016. Inhibition of Ras/Raf/MEK/ERK pathway signaling by a stress-induced phospho-regulatory circuit. Mol. Cell 64, 875–887.
Robey, R.W., Pluchino, K.M., Hall, M.D., Fojo, A.T., Bates, S.E., Gottesman, M.M., 2018. Revisiting the role of ABC transporters in multidrug-resistant cancer. Nat. Rev. Cancer 18, 452–464.

Ruiz, S., Mayor-Ruiz, C., Lafarga, V., Murga, M., Vega-Sendino, M., Ortega, S., Fernandez-Capetillo, O., 2016. A genome-wide CRISPR screen identifies CDC25A as a determinant of sensitivity to ATR inhibitors. Mol. Cell 62, 307–313.
Sanchez-Burgos, L., Navarro-Gonzalez, B., Garcia-Martin, S., Sirozh, O., Mota-Pino, J., Fueyo-Marcos, E., Tejero, H., Anton, M.E., Murga, M., Al-Shahrour, F., Fernandez-Capetillo, O., 2022. Activation of the integrated stress response is a vulnerability for multidrug-resistant FBXW7-deficient cells. EMBO Mol. Med. 14, e15855.
Seo, J.S., Svenningsson, P., 2020. Modulation of ion channels and receptors by p11 (S100A10). Trends Pharm. Sci. 41, 487–497.
Serra, S.A., Stojakovic, P., Amat, R., Rubio-Moscardo, F., Latorre, P., Seisenbacher, G., Canadell, D., Bottcher, R., Aregger, M., Moffat, J., de Nadal, E., Valverde, M.A., Posas, F., 2021. LRRC8A-containing chloride channel is crucial for cell volume recovery and survival under hypertonic conditions. Proc. Natl. Acad. Sci. USA 118.
Shalem, O., Sanjana, N.E., Hartenian, E., Shi, X., Scott, D.A., Mikkelson, T., Heckl, D., Ebert, B.L., Root, D.E., Doench, J.G., Zhang, F., 2014. Genome-scale CRISPR-Cas9 knockout screening in human cells. Science 343, 84–87.
Shekarabi, M., Zhang, J., Khanna, A.R., Ellison, D.H., Delpire, E., Kahle, K.T., 2017. WNK kinase signaling in ion homeostasis and human disease. Cell Metab. 25, 285–299.
Shen, Y., Ori-McKenney, K.M., 2023. Macromolecular crowding tailors the microtubule cytoskeleton through tubulin modifications and microtubule-associated proteins. bioRxiv.
Taieb, H.M., Garske, D.S., Contzen, J., Gossen, M., Bertinetti, L., Robinson, T., Cipitria, A., 2021. Osmotic pressure modulates single cell cycle dynamics inducing reversible growth arrest and reactivation of human metastatic cells. Sci. Rep. 11, 13455.
Tu, S.W., Bugde, A., Luby-Phelps, K., Cobb, M.H., 2011. WNK1 is required for mitosis and abscission. Proc. Natl. Acad. Sci. USA 108, 1385–1390.
Tzelepis, K., Koike-Yusa, H., De Braekeleer, E., Li, Y., Metzakopian, E., Dovey, O.M., Mupo, A., Grinkevich, V., Li, M., Mazan, M., Gozdecka, M., Ohnishi, S., Cooper, J., Patel, M., McKerrell, T., Chen, B., Domingues, A.F., Gallipoli, P., Teichmann, S., Ponstingl, H., McDermott, U., Saez-Rodriguez, J., Huntly, B.J.P., Iorio, F., Pina, C., Vassiliou, G.S., Yusa, K., 2016. A CRISPR dropout screen identifies genetic vulnerabilities and therapeutic targets in acute myeloid leukemia. Cell Rep. 17, 1193–1205.
van Vuuren, R.J., Visagie, M.H., Theron, A.E., Joubert, A.M., 2015. Antimitotic drugs in the treatment of cancer. Cancer Chemother. Pharm. 76, 1101–1112.
Wang, G., Gao, X., Huang, Y., Yao, Z., Shi, Q., Wu, M., 2010. Nucleophosmin/B23 inhibits Eg5-mediated microtubule depolymerization by inactivating its ATPase activity. J. Biol. Chem. 285, 19060–19067.
Wilczynski, B., Dabrowska, A., Saczko, J., Kulbacka, J., 2021. The role of chloride channels in the multidrug resistance. Membranes 12.
Wulff, H., 2008. New light on the "old" chloride channel blocker DIDS. ACS Chem. Biol. 3, 399–401.
Xiao, Y.X., Lee, S.Y., Aguilera-Uribe, M., Samson, R., Au, A., Khanna, Y., Liu, Z., Cheng, R., Aulakh, K., Wei, J., Farias, A.G., Reilly, T., Birkadze, S., Habsid, A., Brown, K.R., Chan, K., Mero, P., Huang, J.Q., Billmann, M., Rahman, M., Myers, C., Andrews, B.J., Youn, J.Y., Yip, C.M., Rotin, D., Derry, W.B., Forman-Kay, J.D., Moses, A.M., Pritisanac, I., Gingras, A.C., Moffat, J., 2024. The TSC22D, WNK, and NRBP gene families exhibit functional buffering and evolved with Metazoa for cell volume regulation. Cell Rep. 43, 114417.
Xiu, M., Li, L., Li, Y., Gao, Y., 2022. An update regarding the role of WNK kinases in cancer. Cell Death Dis. 13, 795.
Xu, B., English, J.M., Wilsbacher, J.L., Stippec, S., Goldsmith, E.J., Cobb, M.H., 2000. WNK1, a novel mammalian serine/threonine protein kinase lacking the catalytic lysine in subdomain II. J. Biol. Chem. 275, 16795–16801.
Xu, B.E., Stippec, S., Lenertz, L., Lee, B.H., Zhang, W., Lee, Y.K., Cobb, M.H., 2004. WNK1 activates ERK5 by an MEKK2/3-dependent mechanism. J. Biol. Chem. 279, 7826–7831.
Yan, V.C., Butterfield, H.E., Poral, A.H., Yan, M.J., Yang, K.L., Pham, C.D., Muller, F.L., 2020. Why great mitotic inhibitors make poor cancer drugs. Trends Cancer 6, 924–941.
Yang, Y.C., Lin, C.H., Lee, E.H., 2006. Serum- and glucocorticoid-inducible kinase 1 (SGK1) increases neurite formation through microtubule depolymerization by SGK1 and by SGK1 phosphorylation of tau. Mol. Cell Biol. 26, 8357–8370.
Ye, T., Mishra, A.K., Banday, S., Li, R., Hu, K., Coleman, M.M., Shan, Y., Chowdhury, S. R., Zhou, L., Pak, M.L., Simone, T.M., Malonia, S.K., Zhu, L.J., Kelliher, M.A., Green, M.R., 2024. Identification of WNK1 as a therapeutic target to suppress IgH/MYC expression in multiple myeloma. Cell Rep. 43, 114211.
Zacco, E., Broglia, L., Kurihara, M., Monti, M., Gustincich, S., Pastore, A., Plath, K., Nagakawa, S., Cerase, A., Sanchez de Groot, N., Tartaglia, G.G., 2024. RNA: the unsuspected conductor in the orchestra of macromolecular crowding. Chem. Rev. 124, 4734–4777.
Zagorska, A., Pozo-Guisado, E., Boudeau, J., Vitari, A.C., Rafiqi, F.H., Thastrup, J., Deak, M., Campbell, D.G., Morrice, N.A., Prescott, A.R., Alessi, D.R., 2007. Regulation of activity and localization of the WNK1 protein kinase by hyperosmotic stress. J. Cell Biol. 176, 89–100.
Zhu, W., Begum, G., Pointer, K., Clark, P.A., Yang, S.S., Lin, S.H., Kahle, K.T., Kuo, J.S., Sun, D., 2014. WNK1-OSR1 kinase-mediated phospho-activation of Na+ -K+ -2Cl- cotransporter facilitates glioma migration. Mol. Cancer 13, 31.